International Journal of Coal Science & Technology (2022) 9:17
https://doi.org/10.1007/s40789-022-00478-0

RESEARCH

Simulation research and application on response characteristics of detecting water-filled goaf by transient electromagnetic method

Tingye Qi[1,2] · Fan Zhang[1,2] · Xiaoming Pei[1,2] · Guorui Feng[1,2] · Huiru Wei[1,2]

Received: 2 June 2021 / Accepted: 17 January 2022

Abstract
Water inrush disasters poses a great threat to the safe exploitation of coal resources. To solve this problem, the transient electromagnetic method (TEM) was proposed to accurately detect the water accumulation in the goaf. The electromagnetic response characteristics of different water-filled goaves were studied by electromagnetic field theory, numerical simulation and field verification. Through the models of 100% water accumulation, 50% water accumulation, 0% water accumulation, 100% water accumulation with collapsed rock, 50% water accumulation with collapsed rock and 0% water accumulation with collapsed rock goaf, the characteristics of induced voltage attenuation curves were studied. Meanwhile, the relationship between the attenuation voltage value and area of the transmitting coil, the depth of the goaf, the background resistivity, and the delay time were also simulated. The results illustrate that the attenuation curve of induced voltage presented a regular exponential decay form in the 0% water accumulation model but existed abnormal exaltation for voltage in water-filled model. Through the linear fitting curve, it can be seen that the abnormal intensity of the induced voltage becomes stronger as the distance between the measuring point and the center of the target decrement. Moreover, the abnormal amplitude of the induced voltage increases with the rise of the water accumulation and collapsed rock will weakly reduce the low-resistivity anomalous effect on the water-accumulated goaf. In addition, the response value of the attenuation voltage increased as the area of the transmitting coil increases, but decreased with increasing delay time and increasing background resistivity and depth of the target body. The field detection results of the Majiliang coal mine also confirmed the theoretical analysis and the numerical simulation.

Keywords Transient electromagnetic method · Water-accumulated goaf · Forward and inverse simulation · Attenuation curve of induced voltage

1 Introduction

In Shanxi Province, China, there has been a large number of private coal mines that have been mining coal for the past few decades. This has led to the existence of many unlocated mine-out areas. Goaf is an enclosed or semi-enclosed area and the overlying strata of the goaf is in an unstable state and may collapse and fall into the goaf. In addition, the enclosed goaf provides storage space for groundwater, so there is often water in the goaf. The water-filled goaf can cause serious accidents and lead to incalculable losses (Hou et al. 2020). In view of this, it is particularly critical to propose a method to accurately locate the mined-out area of coal mine (Wang et al. 2019; Dong 2007). At present, there are many methods for detection. There are a number of methods that can be used to explore the goaf. Among them, the transient electromagnetic method (TEM) has many advantages. When there is water in the goaf, the resistivity of the goaf is lower than the resistivity of the surrounding rocks. Transient electromagnetic method can penetrate high resistivity rock stratum and is sensitive to low resistivity bodies, regardless of terrain (Shan et al. 2009; Liu et al. 2014). Therefore, it is more appropriate to use the TEM to detect the water-filled goaf.

As early as the 1990s, Fitterman et al. (1991) studied the problem of electromagnetic field forward calculation for groundwater exploration and successfully detected

✉ Guorui Feng
fguorui@163.com

[1] College of Mining Engineering, Taiyuan University of Technology, Taiyuan 030024, China

[2] Research Center of Green Mining Engineering Technology in Shanxi Province, Taiyuan 030024, China

Published online: 24 March 2022

groundwater resources on the piedmont alluvial plain in the eastern part of the city of Alain, UAE by using the ground conductivity method and the transient electromagnetic method. Taylor et al. (1992) used transient electromagnetic method to study the characteristics of water system in arid alluvial environment, and characterized the groundwater by the change in color of the apparent resistivity map over time. It can also be used in water accumulation detection. Garg and Keller (1999) proposed a data processing method to obtain a clearer geoelectric structure to determine the location of the water-filled goaf. Finally, applied it to the field detection experiment on the river plain of Idaho Snake. Abu Rajab and El-Naqa (2013) combined the transient electromagnetic method and the DC resistivity sounding method to identify the distribution of freshwater and saline groundwater in the shallow mined-out area in the central Azraq Basin, Jordan. Chang et al. (2019) used the finite-difference time-domain method to calculate the three-dimensional model of the water-filled goaf. The position of the goaf was distinguished by obtaining its full-space transient electromagnetic response characteristics, and the simulation results was verified in a certain mine environment. Li and Liu (2007) obtained the transient electromagnetic response characteristics by analyzing the multichannel voltage map of transient electromagnetic and apparent resistivity map, and accurately detected the location of the multi-layer (water accumulation) mined-out area. Jiang and Yang (2014) studied the transient electromagnetic response characteristics of shallow buried mining areas, and found that when the burial depth was not greater than 100 m. The transient electromagnetic method can effectively identify the goaf with diameter greater than 5 m. High agreement between the results of physical simulation and field measurements. Tang et al. (2015) proposed a transient electromagnetic imaging technology, which detected the area of water accumulation through the two-dimensional apparent resistivity cross-section map and the slice map. The detection example of the water-accumulated goaf in the No. 10 coal seam of Shanxi showed the imaging technology can accurately locate the range and state of the water-filled area. Chang et al. (2017) established a full-space geoelectric model of the mined-out area based on the stratigraphic data in North China and the Middle East. The convolutional perfectly matched layer (CPML) was chosen as the boundary condition and the finite difference time domain method was chosen to simulate the transient electromagnetic response of the coal mine water-bearing collapse column at different depths. Yu et al. (2018) improved the traditional large fixed source loop device of the TEM, and applied it to the detection of the water-filled goaf in Shanxi. The apparent resistivity map was obtained through inversion, and the drilling verification had accurately positioned the buried depth of water-filled goaf. Yan et al. (2020) used electrical source short-offset transient electromagnetic method to detect deep low-resistivity water accumulation areas with buried depth of more than 1000 m. Response characteristics of apparent resistivity and the law of sounding of the H-type theoretical model were obtained by an improved least square method. Moreover, this method was applied to detect the goaf in the deep part of the North China mining area.

In summary, many results have been achieved in the exploration of water-filled goaf by transient electromagnetic methods. However, there are relatively few studies on the characteristics of transient electromagnetic response under complex waterlogging conditions.In this paper, six different states of the goaf are modeled according to the different water content and whether they contain collapse bodies, theoretical analysis and numerical simulation are used to obtain the transient electromagnetic response characteristics of the goaf under different water accumulation conditions, and field tests are performed to verify the simulation results. At the same time, the research results provide theoretical and technical support for the accurate detection of water-filled goaf and coal mine safety production.

2 Theory of transient electromagnetic field for water-filled goaf detection

2.1 Theory of electromagnetic field

Almost all theories of electromagnetic phenomena are derived on the basis of Maxwell's equations. TEM belongs to the time-domain electromagnetic detection method and also complies with the basic equations.

$$\begin{aligned} \nabla \times E &= -\frac{\partial B}{\partial t} \\ \nabla \times H &= j + \frac{\partial D}{\partial t} \\ \nabla \cdot B &= 0 \\ \nabla \cdot D &= \rho \end{aligned} \tag{1}$$

Three matter equations as follow

$$j = \sigma E \quad B = \mu H \quad D = \varepsilon E \tag{2}$$

where E is the electric field intensity (V/m), B is the magnetic induction intensity (Wb/m^2), H is the magnetic field intensity (A/m), D is the electric displacement vector (C/m^2), j is the current density (A/m^2), ρ is the free charge density, σ is the electrical conductivity, μ is the magnetic permeability, and ε is the dielectric constant.

2.2 Calculation of transient electromagnetic field response

According to the relevant studies based on the calculation theory of the electromagnetic field in the frequency domain

(Li 2002; Luo 2012; Bai et al. 2003). The Fourier inverse solution is the best calculation method, so we also conducted calculation theory of the electromagnetic field in the frequency domain and Fourier inverse solution. In order to simplify the calculation process, the cylindrical symmetry of the electromagnetic field is usually chosen to solve the electromagnetic parameters.

Since the electromagnetic field has column symmetry, E has only a component E_φ, H has only the H_r and H_z component, and E, H is independent of the φ, the system of Maxwell's equations can be written in the case of neglecting the displacement current as

$$\begin{aligned} \nabla \times E &= -\frac{\partial B}{\partial t} = -\mu \frac{\partial H}{\partial t} \\ \nabla \times H &= \sigma E \end{aligned} \tag{3}$$

In the cylindrical coordinate

$$\begin{aligned} \nabla \times E = &\left(\frac{1}{r}\frac{\partial E_z}{\partial \varphi} - \frac{\partial E_\varphi}{\partial z}\right) e_r + \left(\frac{\partial E_r}{\partial z} - \frac{\partial E_z}{\partial r}\right) e_\varphi \\ &+ \left(\frac{1}{r}\frac{\partial \left(rE_\varphi\right)}{\partial \varphi} - \frac{1}{r}\frac{\partial E_r}{\partial \varphi}\right) e_z \end{aligned} \tag{4}$$

$$\begin{aligned} \frac{\partial E_\varphi}{\partial z} &= -i\omega\mu H_r \\ \frac{1}{r}\frac{\partial}{\partial r}\left(rE_\varphi\right) &= i\omega\mu H_z \end{aligned} \tag{5}$$

When the mined-out area contains water, the dielectric constant ε, magnetic permeability μ and resistivity ρ will change as follows

$$\varepsilon = \varepsilon_0 \cdot \varepsilon_\mathrm{r} \quad \mu = \mu_0 \cdot \mu_\mathrm{r} \quad \rho_1 = \rho_\mathrm{w} \cdot \frac{3 - w_1}{2w_1} \tag{6}$$

where $\varepsilon_0 = (1/36\pi) \times 10^{-9}$ F/m is the vacuum dielectric constant, ε_r is the relative dielectric constant which depends on the specific rock conditions after water accumulation in the goaf. $\mu_0 = 4\pi \times 10^{-7}$ is the vacuum permeability, μ_r is the relative permeability, ρ_w is the resistivity of water-filled goaf, w_1 is the water content of the rock.

In practical applications, transient electromagnetic instruments generally receive induced electromotive force signals $\varepsilon(t) = \frac{\partial H_z(t)}{\partial t}$. According to the previous calculation method, the following expression is described as

$$\frac{\partial H(\omega)}{\partial t} = -i\omega H_z(\omega) = \frac{3I_0\rho_1}{\mu_0 a^3}\left[1 - \left(1 + k_1 a + \frac{1}{3}k_1^2 a^2\right)e^{-k_1 a}\right] \tag{7}$$

The equation above yields as

$$\begin{aligned} \frac{\partial H_z(t)}{\partial t} = &\frac{3I_0\rho_1}{\mu_0 a^3}\frac{1}{2\pi} \\ &\int_{-\infty}^{\infty}\left[1 - \left(1 + k_1 a + \frac{1}{3}k_1^2 a^2\right)e^{-k_1 a}\right]\frac{e^{-i\omega t}}{-i\omega}\mathrm{d}\omega \end{aligned} \tag{8}$$

After inverse Fourier transform, the equations are

$$\begin{aligned} \frac{\partial H_z(t)}{\partial t} &= \frac{3I_0\rho_\mathrm{w}\left(3 - w_1\right)}{2w_1\mu_0 a^3}\left[\Phi(u) - \sqrt{\frac{2}{\pi}}u\left(1 + \frac{u^2}{3}\right)e^{-\frac{u^2}{2}}\right] \\ &= \frac{3I_0\rho_1}{\mu_0 a^3}f(u) \end{aligned} \tag{9}$$

$$f(u) = \left[\Phi(u) - \sqrt{\frac{2}{\pi}}u\left(1 + \frac{u^2}{3}\right)e^{-u^2/2}\right] \tag{10}$$

where a is the radius of the circular coil (if the transmitting coil is a square coil with side length L, then $a = L/\sqrt{\pi}$), u is the comprehensive parameter, $u = 2\pi a/\tau$, τ is the apparent diffusion parameter, $\tau = 2\pi\sqrt{2\rho t/\mu_0}$, μ_1 is the permeability of the mined-out layer of water, μ_0 is magnetic permeability in vacuum, t is the diffusion time of the transient field, ρ_w is the resistivity of the groundwater goaf.

2.3 Theoretical calculation

MATLAB is used for programming (Tong and Liu 2013) to study the transient electromagnetic response characteristics of the goaf under different water accumulation conditions. The basic parameters are set that the coil radius a is 100 m, the emission current is 1 A. According to the resistivity distribution of the rock stratum in the Majiliang coal mine and some existing studies, the resistivity of the rock around the goaf is set as 500 Ω m, $\mu_0 = 4\pi \times 10^{-7}$ H/m. The resistivity of the mined-out layer are selected as $\rho_1 = 5$ Ω m (fully-water-filled), $\rho_2 = 50$ Ω m (half-water-filled), and $\rho_3 = 1000$ Ω m (water-unfilled) respectively and the burial depth of the goaf is 50 m, the length and width of the goaf are 100 m and the thickness is 10 m and t is the diffusion time, ranging from 0.01 to 0.1 ms. The coordinate axis is expressed in double logarithmic form, and the attenuation voltage curves under the three models are shown in Fig. 1.

The attenuation trend of the three curves is similar and the attenuation voltage response value is proportional to the amount of water accumulation. It also shows that the greater the amount of water accumulation, the higher the voltage value.

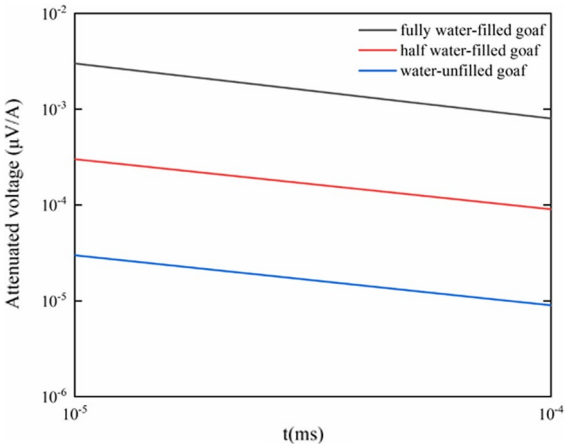

Fig. 1 Attenuated voltage curve of the water-filled goaf under different states

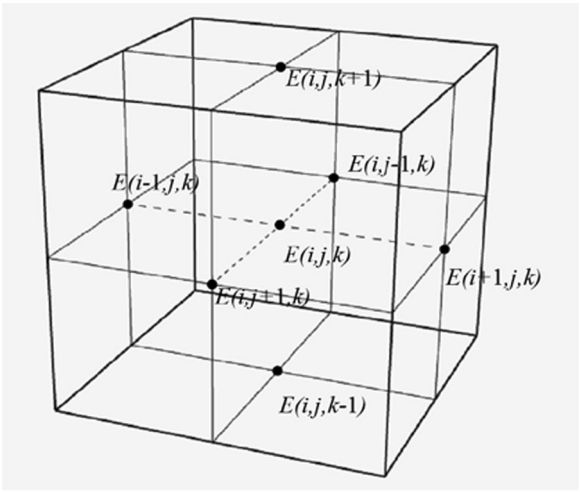

Fig. 2 Finite time domain differential cubic unit

3 Numerical simulation of transient electromagnetic response of water-filled goaf in different states

3.1 Goaf model of water-filled states

Coal mine goaf is the closed or semi-enclosed space area left behind by the underground coal seam being mined. After the goaf formed, the integrity of the rock strata is destroyed, causing a large area of cracks inside the rock strata. When the goaf is filled with water, its resistivity is lower than the surrounding rock. When the goaf does not contain water, the resistivity of the goaf is higher than the resistivity of the surrounding rock. Simulation research is carried out based on the physical characteristics (Han 2018; Lian et al. 2020). The resistivity of the goaf is higher than the surrounding rock. The simulation was used Maxwell software for calculation. In order to truly reflect the changes in the water environment in the mined-out area, the plate-shaped structure was selected to simulate the various underground rock layers and 6 goaf models of 100% water accumulation, 50% water accumulation, 0% water accumulation, 100% water accumulation with collapsed rock, 50% water accumulation with collapsed rock and 0% water accumulation with collapsed rock were established. Then the electromagnetic response characteristics were analysed through the attenuation electromotive force curve and apparent resistivity cross-section obtained by forward and inversion simulation.

In this study, the water-accumulating goaf of Majiliang mining area in Datong is selected as the research object, the forward model is established by referring to the site geological conditions and the electrical properties of the overlying rock and floor layer of the goaf.

3.2 Three-dimensional forward principle

The 3D time-domain finite-difference algorithm is used for forward simulation. The set of Maxwell's equations in the right-angle coordinate system is

$$\begin{aligned}\frac{\partial E_z}{\partial y}-\frac{\partial E_y}{\partial z}&=-\frac{\partial B_x}{\partial t}\\ \frac{\partial E_x}{\partial z}-\frac{\partial E_z}{\partial x}&=-\frac{\partial B_y}{\partial t}\\ \frac{\partial E_y}{\partial x}-\frac{\partial E_x}{\partial y}&=-\frac{\partial B_z}{\partial t}\end{aligned}\tag{11}$$

$$\begin{aligned}\frac{\partial H_z}{\partial y}-\frac{\partial H_y}{\partial z}&=\gamma\frac{\partial E_x}{\partial t}+\sigma E_x\\ \frac{\partial H_x}{\partial z}-\frac{\partial H_z}{\partial x}&=\gamma\frac{\partial E_y}{\partial t}+\sigma E_y\\ \frac{\partial H_y}{\partial x}-\frac{\partial H_x}{\partial y}&=\gamma\frac{\partial E_z}{\partial t}+\sigma E_z\end{aligned}\tag{12}$$

$$\nabla\times\nabla\times E=\nabla\nabla\cdot E-\nabla^2 E\tag{13}$$

The above equations lead to the diffusion equation of the electric field. The solution area is non-uniformly meshed in three dimensions, thus transforming the infinite computational area into a solved small rectangular cell as shown in Fig. 2. The continuous electric field is replaced by the discrete electric field of each node, and the cubic cell is constructed with any node and other nodes adjacent to it.

$$E^{n+1}(i,j,k) = \frac{1}{R(i,j,k)}\left[A^{'}(i,j,k)E^{n-1}(i,j,k) + A_1^{'}(i,j,k)E^{n}(i+1,j,k) + A_2^{'}(i,j,k)E^{n}(i-1,j,k) + A_3^{'}(i,j,k)E^{n}(i,j+1,k) + A_4^{'}(i,j,k)E^{n}(i,j-1,k) + A_5^{'}(i,j,k)E^{n}(i,j,k+1) + A_6^{'}(i,j,k)E^{n}(i,j,k-1)\right] \tag{14}$$

$$\mu\left(\partial H_z/\partial t\right) = \left(\partial E_x/\partial y\right) - \left(\partial E_y/\partial x\right) \tag{15}$$

$$B(i,j,k) = \frac{\mu}{8}\left[\sigma(i,j,k)\Delta x_i\Delta y_j\Delta z_k + \sigma(i+1,j,k)\Delta x_{i+1}\Delta y_j\Delta z_k + \sigma(i,j+1,k)\Delta x_i\Delta y_{j+1}\Delta z_k + \sigma(i,j,k+1)\Delta x_i\Delta y_j\Delta z_{k+1} + \sigma(i+1,j+1,k)\Delta x_{i+1}\Delta y_{j+1}\Delta z_k + \sigma(i,j+1,k+1)\Delta x_i\Delta y_{j+1}\Delta z_{k+1} + \sigma(i+1,j,k+1)\Delta x_{i+1}\Delta y_j\Delta z_{k+1} + \sigma(i+1,j+1,k+1)\Delta x_{i+1}\Delta y_{j+1}\Delta z_{k+1}\right] \tag{16}$$

$$\begin{aligned} R(i,j,k) &= B(i,j,k) - A(i,j,k)\Delta t \\ A^{'}(i,j,k) &= B(i,j,k) + A(i,j,k)\Delta t \\ A_n^{'}(i,j,k) &= 2A_n(i,j,k)\Delta t \end{aligned} \tag{17}$$

In order to ensure the stability of the calculation, the time increment and space increment in the time domain finite difference satisfy Eq. (18), V is the speed of propagation of electromagnetic waves.

$$V\Delta t \le \left(\frac{1}{\Delta x^2} + \frac{1}{\Delta y^2} + \frac{1}{\Delta z^2}\right)^{-1/2} \tag{18}$$

Finally, Mur absorption boundary conditions are used to handle the nodes on the boundary.

3.3 Transient electromagnetic response characteristics of goaf models in different water-accumulated states

The detection coil is selected centre loop coil and basic parameters of the model have been set after several tests. The emission current is 1 A, the transmission frequency is 8 Hz, the turn number is 1, the side length of the transmitting coil is 100 m, and the receiving device selects a probe with an equivalent area of 10,000 m^2. Moreover, the sampling time is 27 ms, the number of channels is 27, and the amounts of measuring lines and points are 1 and 21 respectively. The distance between the measuring points is 25 m. The total latera measured distance ranges from 0 to 500 m. Each plate-shaped body is centred at a lateral position of 250 m.

Figure 3a shows the schematic diagram of the model of the 100% water accumulation goaf. According to the buried depth from shallow to deep, it is divided into three layers of geological bodies called overlying rock layer, water-filled goaf layer, and floor layer, corresponding to the resistivity of each layer is 1000, 5 and 200 Ω m, the thickness is 100, 20 and 50 m respectively and the length is 200 m, the width is 200 m. The rest of the space is considered as the surrounding rock, the resistivity is 500 Ω m while the thickness is infinite, and the subsequent models are also the same.

Figure 3b shows the schematic diagram of the model of the 50% water accumulation goaf. According to the buried depth from shallow to deep, it is divided into four layers of geological bodies called overlying rock layer, goaf layer, water-filled goaf layer, and floor layer, corresponding to the resistivity of each layer is 1000, 2000, 5 and 200 Ω m, the thickness is 100, 10, 10 and 50 m respectively and the length is 200 m, width is 200 m.

Figure 3c shows the schematic diagram of the model of the 0% water accumulation goaf. According to the buried depth from shallow to deep, it is divided into three layers of geological bodies called overlying rock layer, goaf layer, and floor layer, corresponding to the resistivity of each layer is 1000, 2000 and 200 Ω m, the thickness is 100, 20 and 50 m respectively and the length is 200 m, width is 200 m.

Figure 3d shows the model diagram of the 100% water accumulation with collapsed rock. It is divided into three geological bodies of overlying rock layer, water-filled goaf layer and floor layer according to the buried depth from shallow to deep, corresponding to the resistivity of each layer is 1000, 5 and 200 Ω m, the thickness is 100, 20 and 50 m respectively and the length is 200 m, the width is 200 m. The collapsed rock exists in the mined-out area which is set the length of 50 m and thickness of 10 m, and the resistivity of the collapsed rock mass is 1000 Ω m.

Figure 3e shows the model diagram of the 50% water accumulation with collapsed rock. It is divided into four geological bodies of overlying rock layer, goaf layer, water-filled goaf layer and floor layer according to the buried depth from shallow to deep, corresponding to the resistivity of each layer is 1000, 2000, 5 and 200 Ω m, the thickness is 100, 10, 10 and 50 m respectively and the length is 200 m, the width is 200 m.

Figure 3f shows the model diagram of the 0% water accumulation with collapsed rock. It is divided into three geological bodies of overlying rock layer, goaf layer and floor layer according to the buried depth from shallow to deep, corresponding to the resistivity of each layer is 1000, 2000 and 200 Ω m, the thickness is 100, 20 and 50 m respectively and the length is 200 m, the width is 200 m.

According to the forward simulation calculation, the attenuation voltage curve of each model is obtained to reflect the transient electromagnetic response characteristics. The

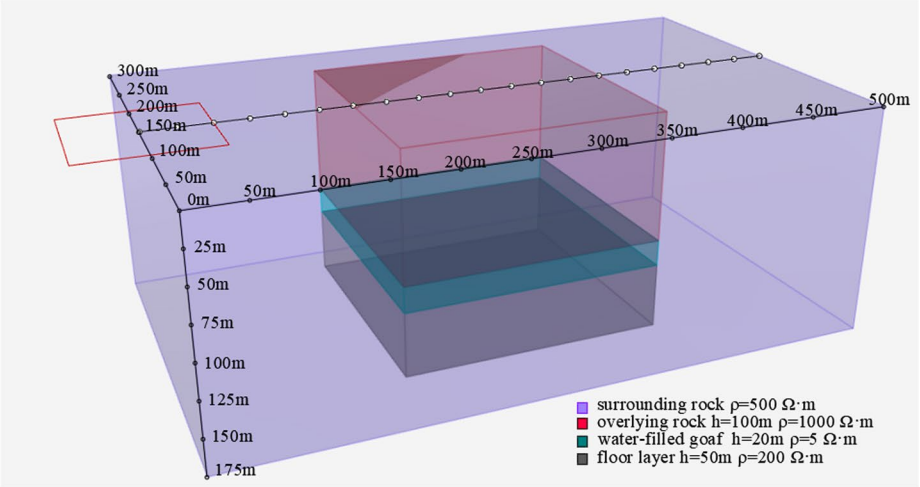

(a)

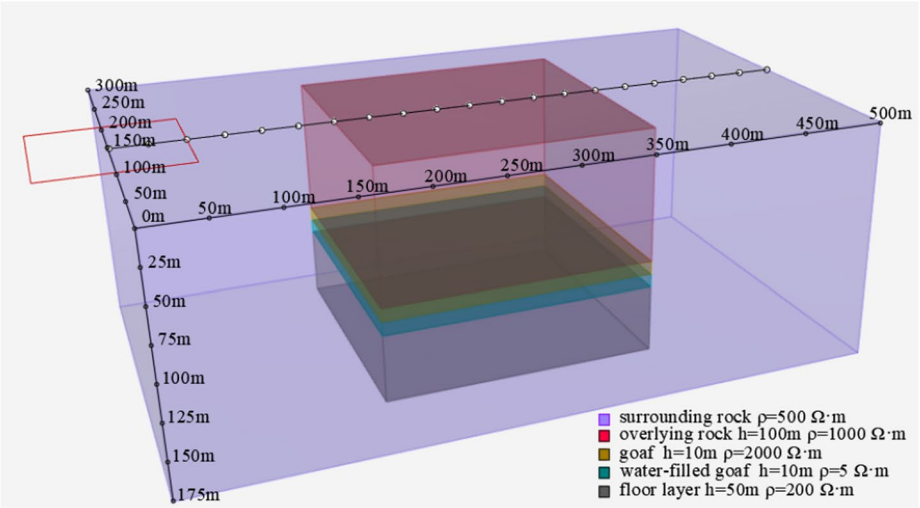

(b)

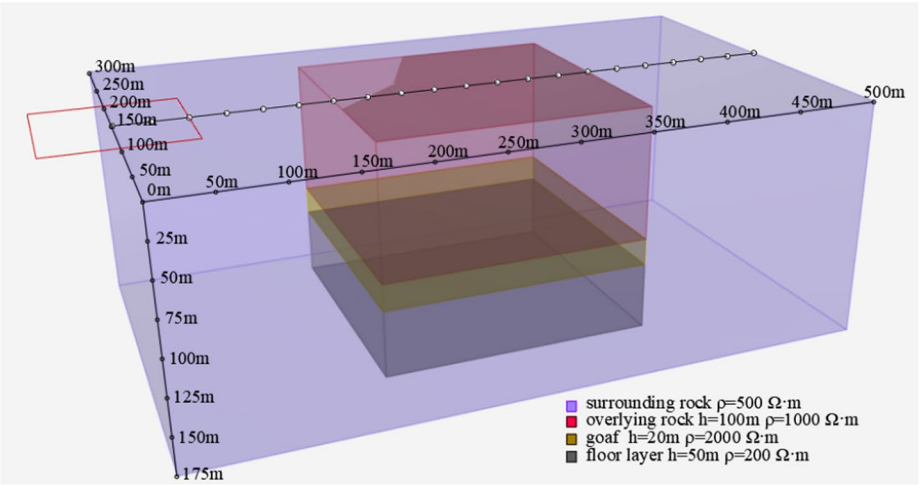

(c)

Fig. 3 Model of the water-filled goaf under different states: **a** Model of the 100% water accumulation goaf; **b** Model of the 50% water accumulation goaf; **c** Model of the 0% water accumulation goaf; **d** Model of the 100% water accumulation with collapsed rock goaf; **e** Model of the 50% water accumulation with collapsed rock goaf; **f** Model of the 0% water accumulation with collapsed rock goaf

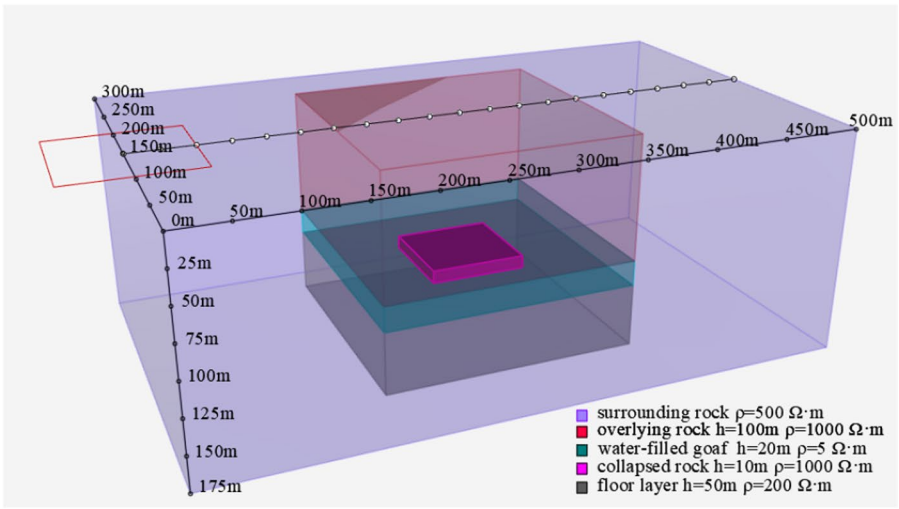

(d)

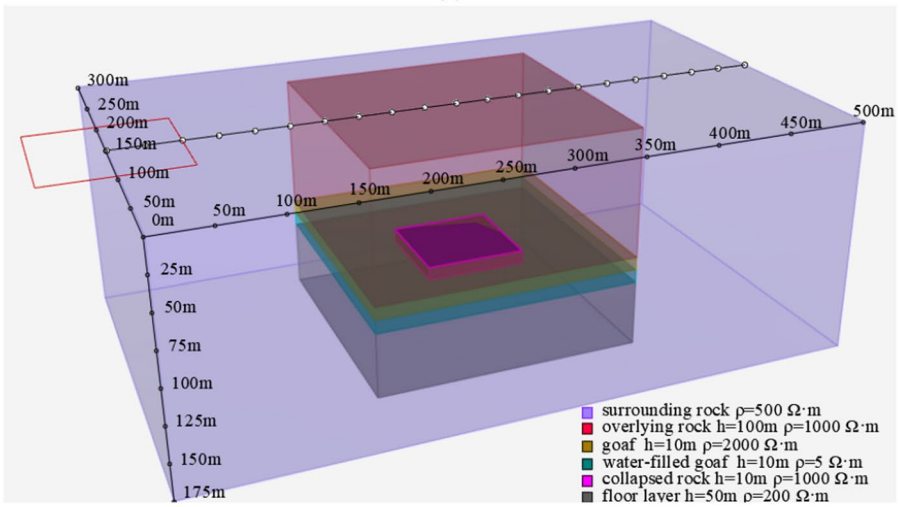

(e)

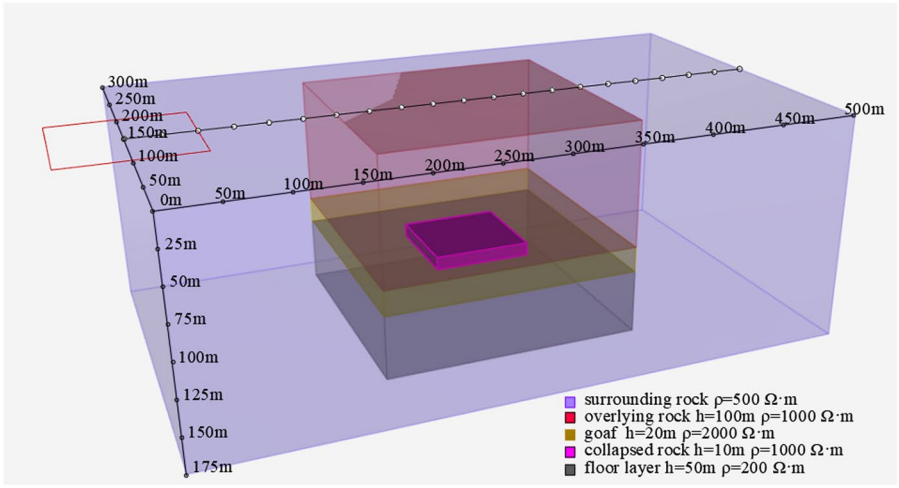

(f)

Fig. 3 (continued)

curve was expressed in double logarithmic coordinates, the ordinate is the normalized attenuation voltage response value, and the abscissa is the delay time. In order to clearly reflect the response characteristics, we select the six points at the horizontal distance of 50, 100, 125, 150, 175 and 250 m on the survey line to observe.

The attenuation voltage curves of the six conditions of water accumulation were selected. The voltage curve will show obvious "bulge" abnormal reflection when goaf contains water, and the shape presents "S" type. The closer the measurement point is to the upper part of the water in the goaf, the more obvious the abnormal response, which indicates that TEM has a stronger ability to distinguish relatively low-resistivity anomalies containing water, as shown in Fig. 4a and b. The voltage curves almost overlap when the goaf is water-unfilled, the attenuation trend is similar, and the curve presents the characteristics of an exponential attenuation curve that indicates TEM has no obvious abnormal response to the unfilled relatively high-resistivity target, as shown in Fig. 4c. The collapsed rock is formed by the landsliding of the roof, and its resistivity is relatively high compare to the surrounding rock. If water and collapsed bodies both contain in the mined-out area, the attenuation curve still produces a relatively large "bulge" anomaly. However, the abnormal response is weakened, and the voltage value is correspondingly reduced. It can be known that when the water and the collapsed body exist at the same time, the impact of the water on the attenuation voltage response is more significant, and the collapsed body can only reduce the abnormal amplitude, as shown in Fig. 4d and e. When the goaf has collapsed rock with 0% water accumulation, the target body shows relatively high-resistivity, and the attenuation voltage curve is not abnormal. The attenuation trend of curve is consistent with the water-unfilled goaf model, as shown in Fig. 4f.

Linear fitting is performed for the attenuation voltage curve of the above water accumulation model, taking the 100% water accumulation mined-out area as an example, the fitted curve is shown in Fig. 5. The measurement point 250 is directly above the goaf, the smaller the measurement point number the further away from the goaf. It can be seen from the figure that all the fitted curves are in a linear function distribution, and the slope of the curve increases with the increment of the number of measuring points, while the fit degree of the curve becomes worse, and the R^2 value continues to decrease. When the measuring point distance is 250 m, the R^2 value is only 0.97873. It indicates that the attenuation curve located in the center of the water-filled goaf has the strongest anomalous response.

According to the attenuated voltage response of the forward modeling, the apparent resistivity profile diagrams of six types of water-filled goafs were obtained by inversion calculation. Although 2-D and 3-D inversions have been proposed, 1-D inversions are more popular. The Maxwell software-based EMAX program performs inversion calculations of apparent resistivity and apparent depth for different states of the mined area. The inversion program is based on Occam's algorithm (Constable et al. 1987). There is an inverse proportional relationship between the apparent resistivity value and the induced electromotive force response value. The abscissa shows the lateral distance position of the measuring point, and the ordinate shows the depth of burial. The colorimetric scale chart below shows the apparent resistivity value and color deepens and increases continuously as shown in Fig. 6.

When the goaf is completely filled with water, a relatively low-apparent resistivity enclosed area appears at the buried depth of −100 m to −130 m and the measuring point distance of 150–350 m (water-filled goaf). The abnormal increment for the induced electromotive force lead to the decrement of apparent resistivity value when the goaf is fully water-filling. Corresponding to the above-mentioned forward modeling results, the apparent resistivity contour lines around are distributed in irregular shapes, as shown in the Fig. 6a. When the goaf contains 50% water, the relatively high-resistivity air layer will weaken the abnormal amplitude. Compared with the full-water model, a small anomaly relatively low-apparent resistivity enclosed area will generate at the buried depth −105 m to −120 m and the lateral distance from 175 to 330 m, as shown in Fig. 6b. When there is no water in the mined-out area, no obvious enclosed area appears on the apparent resistivity profile diagram, the apparent resistivity of each layer is linearly distributed, and the value is high. This is because the induced electromotive force does not increase abnormally, while the apparent resistivity value did not decrease significantly, as shown in Fig. 6c.

For the mined-out area with collapsed rock mass, based on the slight difference of the induced voltage response, and the trend of the apparent resistivity profile obtained from the inversion is some different from mind-out area without collapsed rock. The apparent resistivity value has little increment.

To analyze the influence of three states for 100% water accumulation goaf, 50% water accumulation goaf and water-unfilled goaf on the voltage response value, we selected the attenuation curve generated at the measurement point (250 m) with the strongest response characteristic for analysis.

The attenuation voltage curve under different water accumulation conditions is shown in Fig. 7. The response value of the attenuation voltage depends on the resistivity value of the stratum at different buried depths. Since the overburden setting of each model is the same, the initial response values of the three goaf models under the conditions of water accumulation are basically analogous. Afterwards, due to

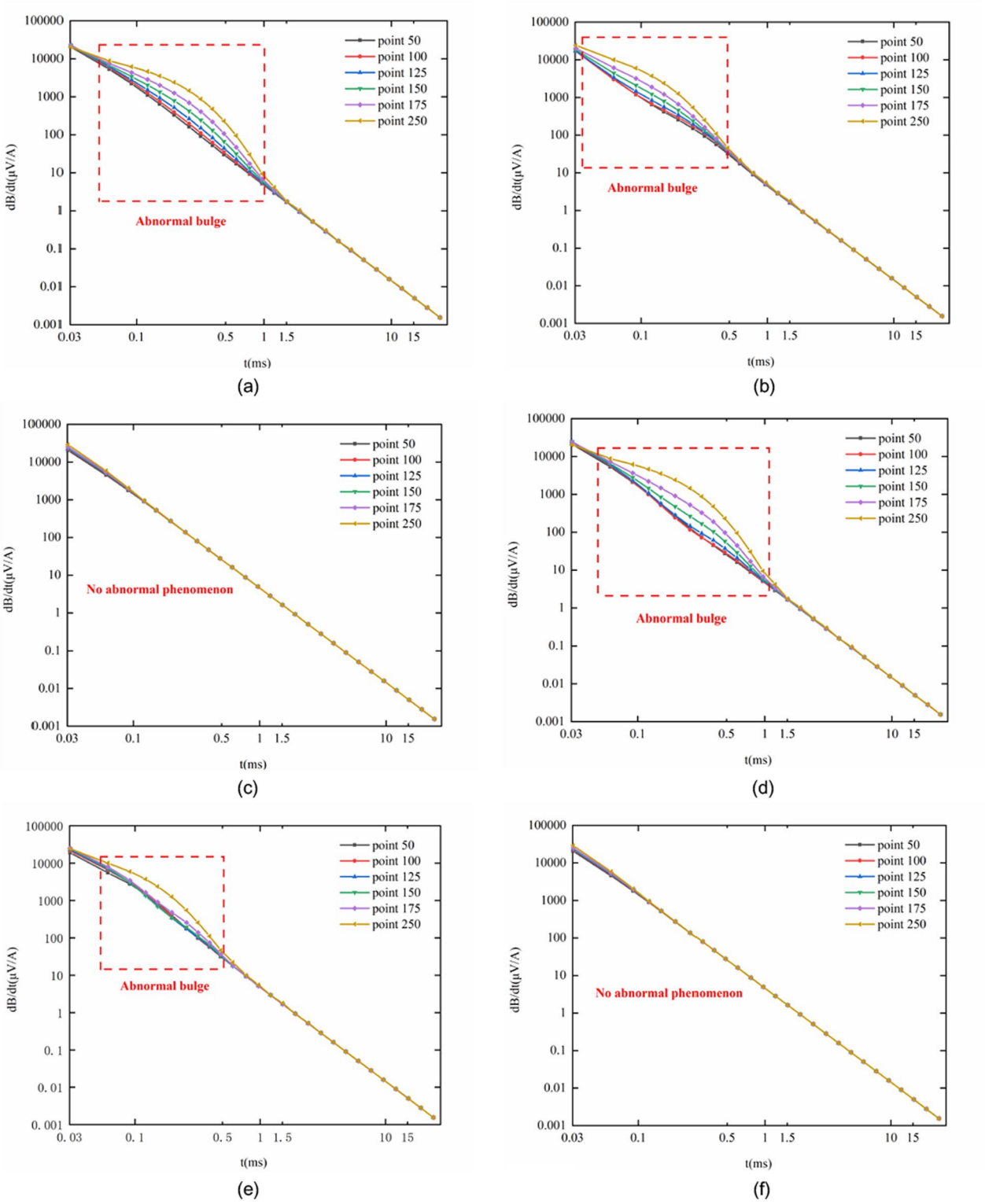

Fig. 4 Attenuated voltage curve of water-filled goaves in different states: **a** Model of the 100% water accumulation goaf; **b** Model of the 50% water accumulation goaf; **c** Model of the 0% water accumulation goaf; **d** Model of the 100% water accumulation with collapsed rock goaf; **e** Model of the 50% water accumulation with collapsed rock goaf; **f** Model of the 0% water accumulation with collapsed rock goaf

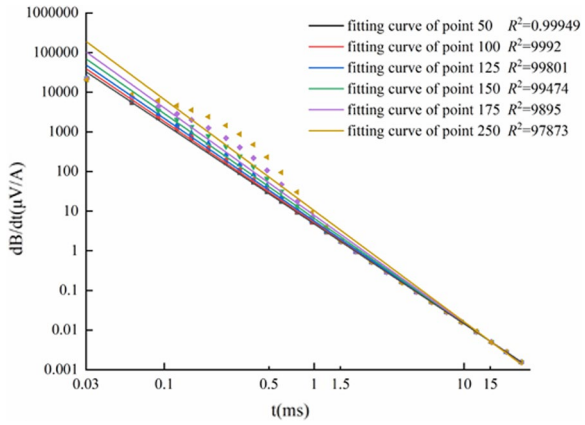

Fig. 5 Fitting curve of the attenuation voltage of measuring points in 100% water accumulation goaf

the low resistivity characteristics of the water accumulation, the induced voltage curve will produce abnormal "bulge" phenomenon. The attenuation process is limited and the sequence of the degree of abnormal response is 100% water accumulation goaf > 50% water accumulation goaf > 0% water accumulation goaf. Which implies that the larger the amount of water accumulation, and brought the more obvious the low resistivity effect. Moreover, the rate of attenuation of the induced electromotive force response is slower while the response value is higher.

3.4 Transient electromagnetic response characteristics of water-filled goaf with different coil sizes

This section studies the electromagnetic response characteristics of six goaf models under different transmitter coil sizes. The working parameters are set as follows: the emission current is 1 A, the delay time is 0.01 ms, the emission frequency is 8 Hz, the number of turns is 1, the background resistivity is 500 Ω m, the sampling time is 27 ms, and the number of time channels is 27. The side lengths of the single-turn transmitting coils is set as 100, 150, 200, 300 and 400 m respectively, and the receiving coils were selected with an equivalent area of 10,000 m^2 to perform forward calculations on each goaf model, as shown in Fig. 8.

As can be seen from the figure, regardless of the water content of the goaf, regardless of the presence of collapse bodies in the goaf, the attenuation voltage value increases with the increase of the side length of the transmitting coil in both the early middle and late stages of the attenuation voltage curve. However, the amplification of the attenuation voltage value decreases with the increase of the side length of the transmitting coil when there is water in the goaf as shown in Fig. 8a, b, d and e. In addition, as the side length of the transmitting coil increases, the low resistivity abnormal bulge in the attenuation voltage curve becomes not obvious.

In order to obtain the relationship between the coil side length and the attenuation voltage value, the voltage values were chosen at the first, second, sixth and seventh measurement channels, where the first and second measurement channels are before the abnormal response time, and the sixth and seventh measurement channels are within the abnormal response time to fit the relationship between the two. The corresponding fitting curve is shown in Fig. 9.

The results show that the attenuation voltage response values corresponding to the six types of mined-out areas all increase. But the corresponding voltage increases faster with the increase of the side length of the transmitting coil when there is no water accumulation in the mined-out areas as shown in Fig. 9c and f. An increase in the side length of the transmitting coil increases the low resistivity abnormal bulge in the attenuation voltage curve, but increases the response voltage value of the entire stratum even more. This is why the low resistivity abnormal bulge in the attenuation voltage curve becomes not obvious as the coil side length increases. In addition, for six types of mined-out areas, the increase in the side length of the transmitting coil increases the response voltage value of the early measurement channel even more.

3.5 Transient electromagnetic response characteristics of water-filled goaf under different buried depths

This section studies the electromagnetic response characteristics of six goaf models under different buried depths. The working parameters are set as follows: the emission current is 1 A, the delay time is 0.01 ms, the emission frequency is 8 Hz, the number of turns is 1, the background resistivity is 500 Ω m, the sampling time is 27 ms, and the number of time channels is 27. We chose a 100 m × 100 m square coil for the transmitting coil, and a probe with an equivalent area of 10,000 m^2 for the receiving coil. The buried depth of the water-filled goaf is set to 50, 100, 150, 200 and 250 m respectively to perform forward calculations on each goaf model, as shown in Fig. 10.

It can be seen that the depth of the goaf has very little effect on the attenuation voltage curve when there is no water in the extraction area, as shown in Fig. 10c and f. However when there is water in the goaf, the burial depth of the goaf has a very big influence on the voltage attenuation curve. In addition, with the increase of water accumulation in the goaf, the influence of the burial depth of the goaf on the voltage attenuation curve increases.as shown in Fig. 10a, b, d and e. When there is water in the goaf, as the burial depth of the goaf increases, the appearance of the bulge anomaly of the voltage attenuation curve is delayed, the magnitude of the bulge anomaly is weakened, and the

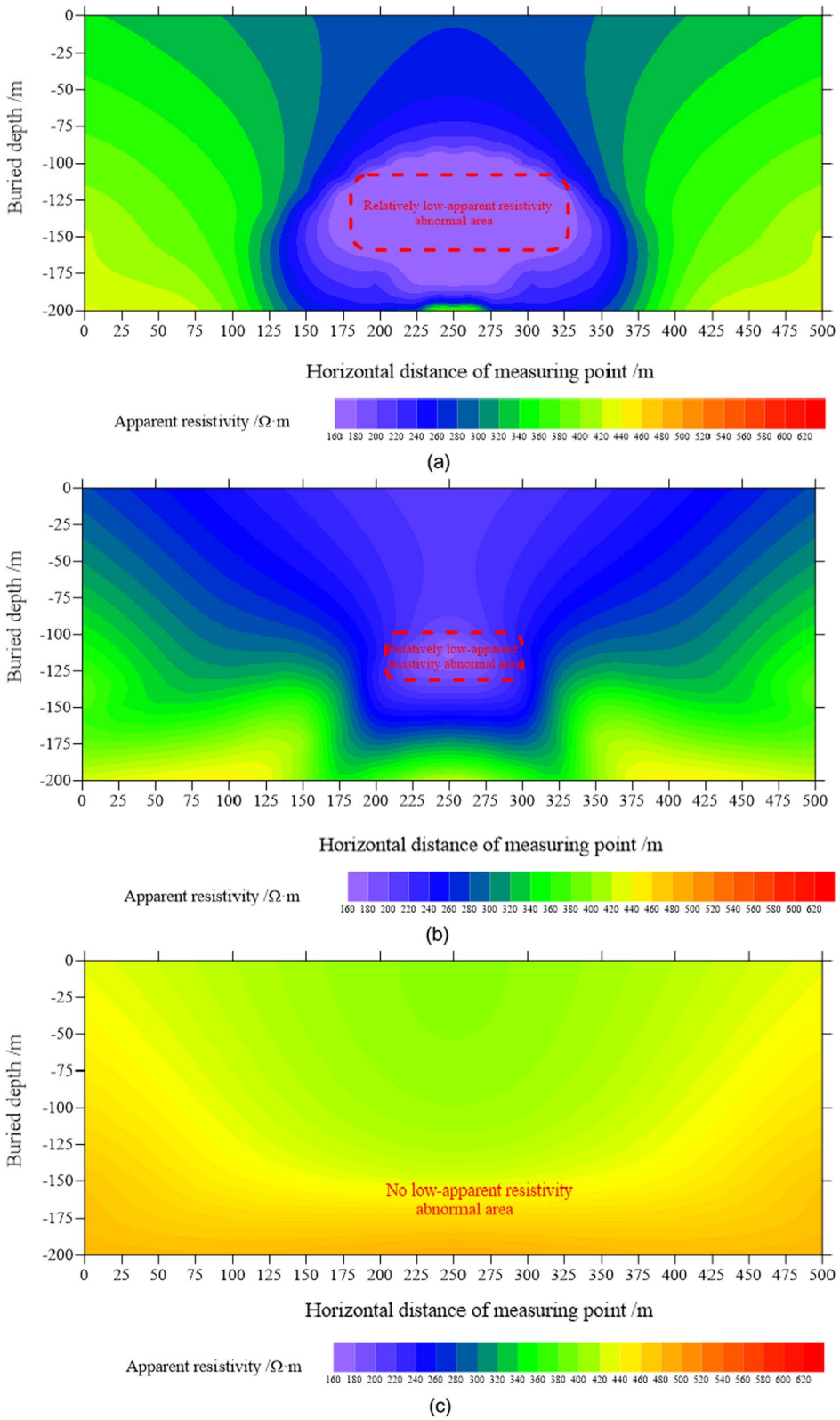

Fig. 6 The apparent resistivity cross-section diagrams of the goaf with water accumulation in different states: **a** Model of the 100% water accumulation goaf; **b** Model of the 50% water accumulation goaf; **c** Model of the 0% water accumulation goaf; **d** Model of the 100% water accumulation with collapsed rock goaf; **e** Model of the 50% water accumulation with collapsed rock goaf; **f** Model of the 0% water accumulation with collapsed rock goaf

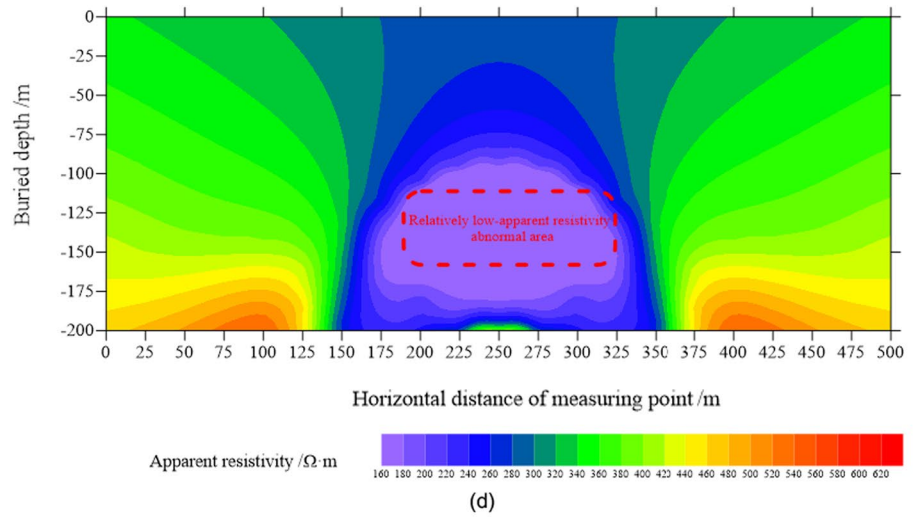

(d)

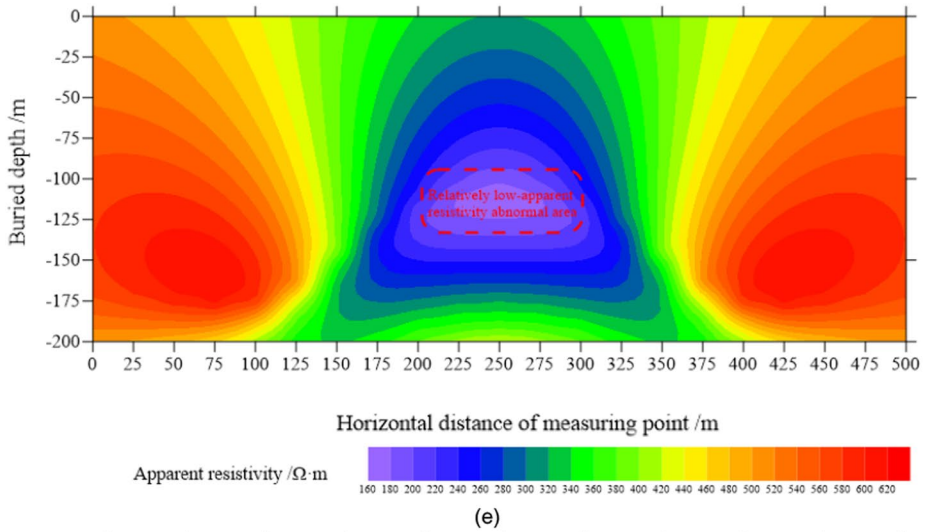

(e)

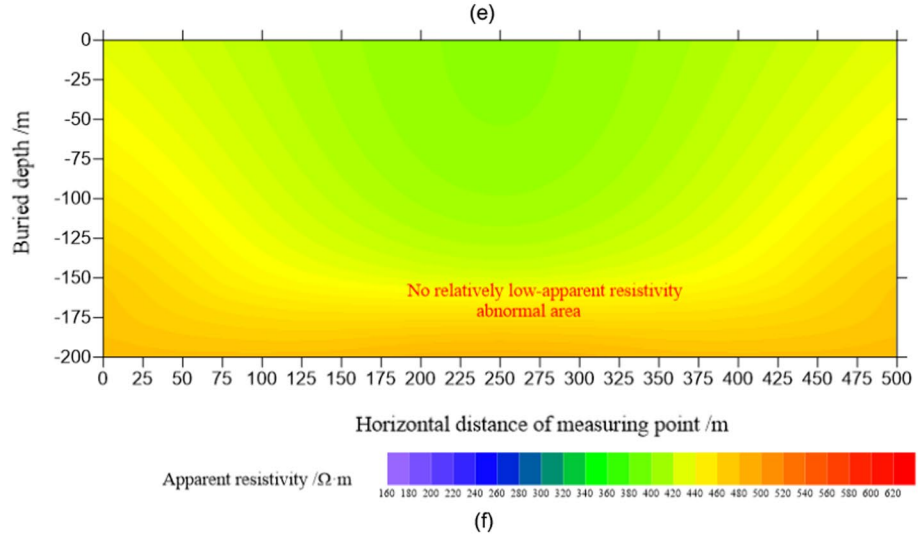

(f)

Fig. 6 (continued)

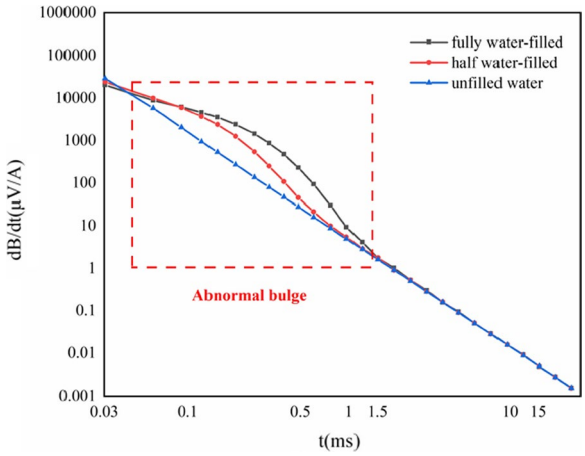

Fig. 7 Attenuation voltage curves under different amounts of accumulated water

duration of the bulge anomaly is shortened. There is almost no difference between voltage attenuation curve of the water-accumulating goaf and the voltage attenuation curve of the goaf without water accumulation, when the burial depth of the goaf increases to 250 m. This is because the intensity of the transient electromagnetic field signal gradually weakens when it penetrates the rock formations, and the ability to interpret low resistivity anomalies will continue to decrease as the depth increases. The above results indicate that the transient electromagnetic exploration has limited detection capabilities for abnormal objects, and detecting deeper mining areas, it is necessary to adjust some parameters.

In order to obtain the relationship between the buried depth and the attenuation voltage value, the first, second, sixth and seventh measurement channels of voltage values were selected to fit the relationship between the two, and the corresponding fitting curve is shown in Fig. 11.

The results show that when there is no water in the goaf, the increase of the burial depth of the goaf has little effect on the response voltage values of the first and second measurement channels, as shown in Fig. 11c and f. However, when there is water in the goaf, the depth of burial of the goaf varies from 50 to 100 m, which has a greater impact on the response voltage values of the first and second measurement channels, and a relatively small impact on the sixth and seventh measurement channels as shown in Fig. 11a, b, d and e. This is because the temporal electromagnetic fields corresponding to the first and second channels are still present at shallow burial depths, and the corresponding voltages at this time only reflect information from the shallow part of the strata. For the buried deeper goaf, we should pay attention to the later measurement channel.

3.6 Transient electromagnetic response characteristics of water-filled goaf with different background resistivity

This section studies the electromagnetic response characteristics of six goaf models with different background resistivity. The working parameters are set as follows: the emission current is 1 A, the delay time is 0.01 ms, the emission frequency is 8 Hz, the number of turns is 1, the sampling time is 27 ms, and the number of time channels is 27, the buried depth of the water-filled goaf is 100 m.We choose a 100 m × 100 m square coil for the transmitting coil, and a probe with an equivalent area of 10,000 m^2 for the receiving coil. The background resistivity is set to 500, 1000, 1500, 2000 and 3000 Ω m to perform forward calculations on each goaf model, as shown in Fig. 12.

As can be seen from the figure, when there is water accumulation in the goaf, the abnormal bulge of the attenuation voltage curve becomes more obvious with the increase of the background resistivity, and the duration of the abnormal bulge increases. This is because the increase in the resistivity of the background leads to an increase in the difference between the resistivity of the goaf and the resistivity of the background, making the low resistivity response of the goaf more obvious. In addition, the increase in background resistivity will reduce the quality of the attenuation voltage curve in the goaf, and fluctuations in the attenuation voltage curve will occur in the late stage as shown in Fig. 12a, b, d and e. When there is no water in the goaf, an increase in the background resistivity only decreases the overall response value of the attenuation voltage curve as shown in Fig. 12c and f.

In order to obtain the relationship between the background resistivity and the attenuation voltage value, the second, sixth, seventh and fifteenth measurement channels of voltage values were selected to fit the relationship between the two, and the corresponding fitting curve is shown in Fig. 13.

From Fig. 13, it can be seen that the increase in background resistivity has a greater effect on the attenuation voltage value of the second channel, while the effect on the other three channels is smaller. When there is no water in the goaf, the attenuation voltage value of the second measurement channel decreases with the increase of the background resistivity as shown in Fig. 13c and f, while when there is water in the goaf, the change of the background resistivity has less effect on the attenuation voltage value, as shown in Fig. 13a, b, d and e. This is because the studied measurement point

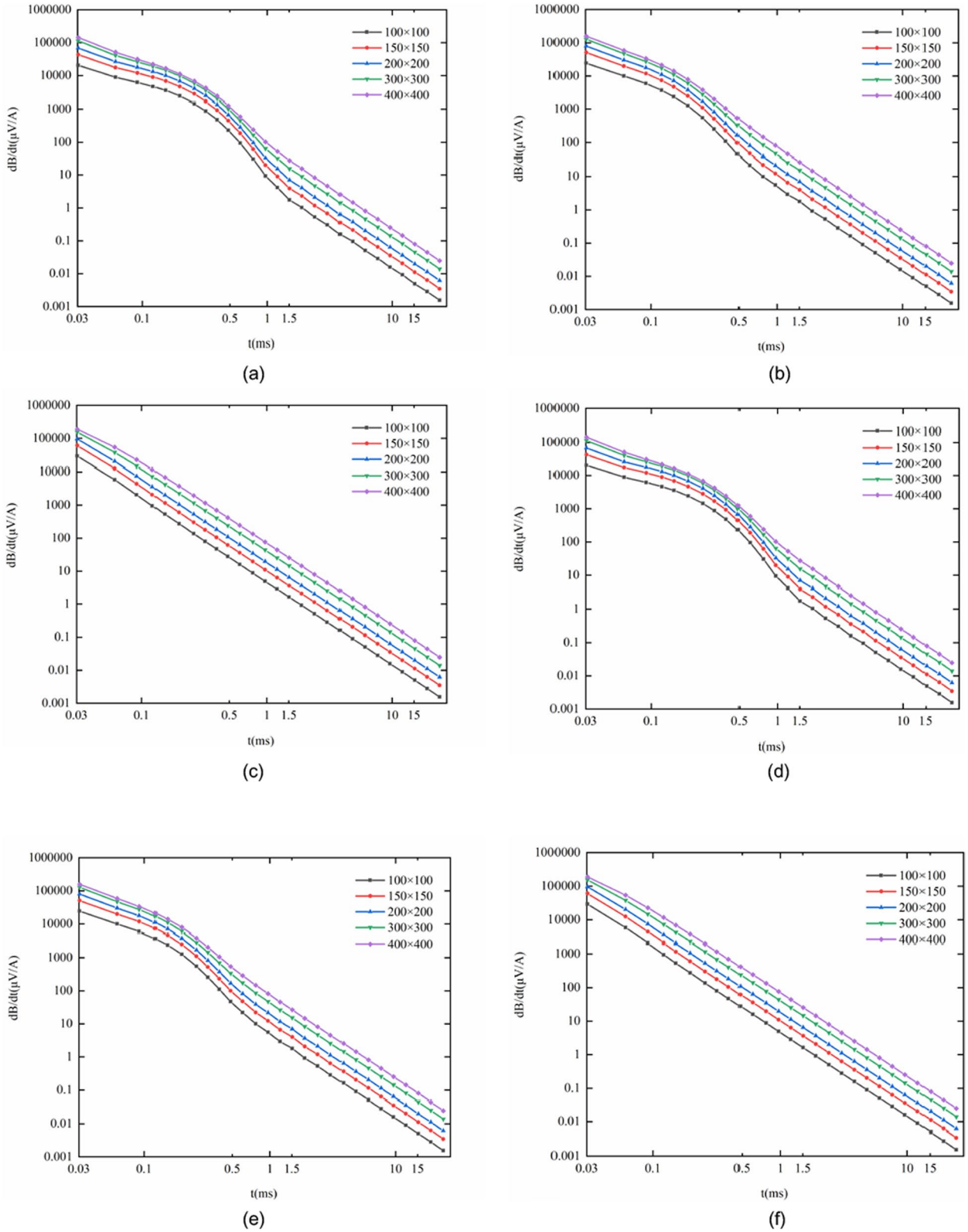

Fig. 8 Attenuated voltage curves of the different water-filled goaf models with different coil sizes: **a** Model of the 100% water accumulation goaf; **b** Model of the 50% water accumulation goaf; **c** Model of the 0% water accumulation goaf; **d** Model of the 100% water accumulation with collapsed rock goaf; **e** Model of the 50% water accumulation with collapsed rock goaf; **f** Model of the 0% water accumulation with collapsed rock goaf

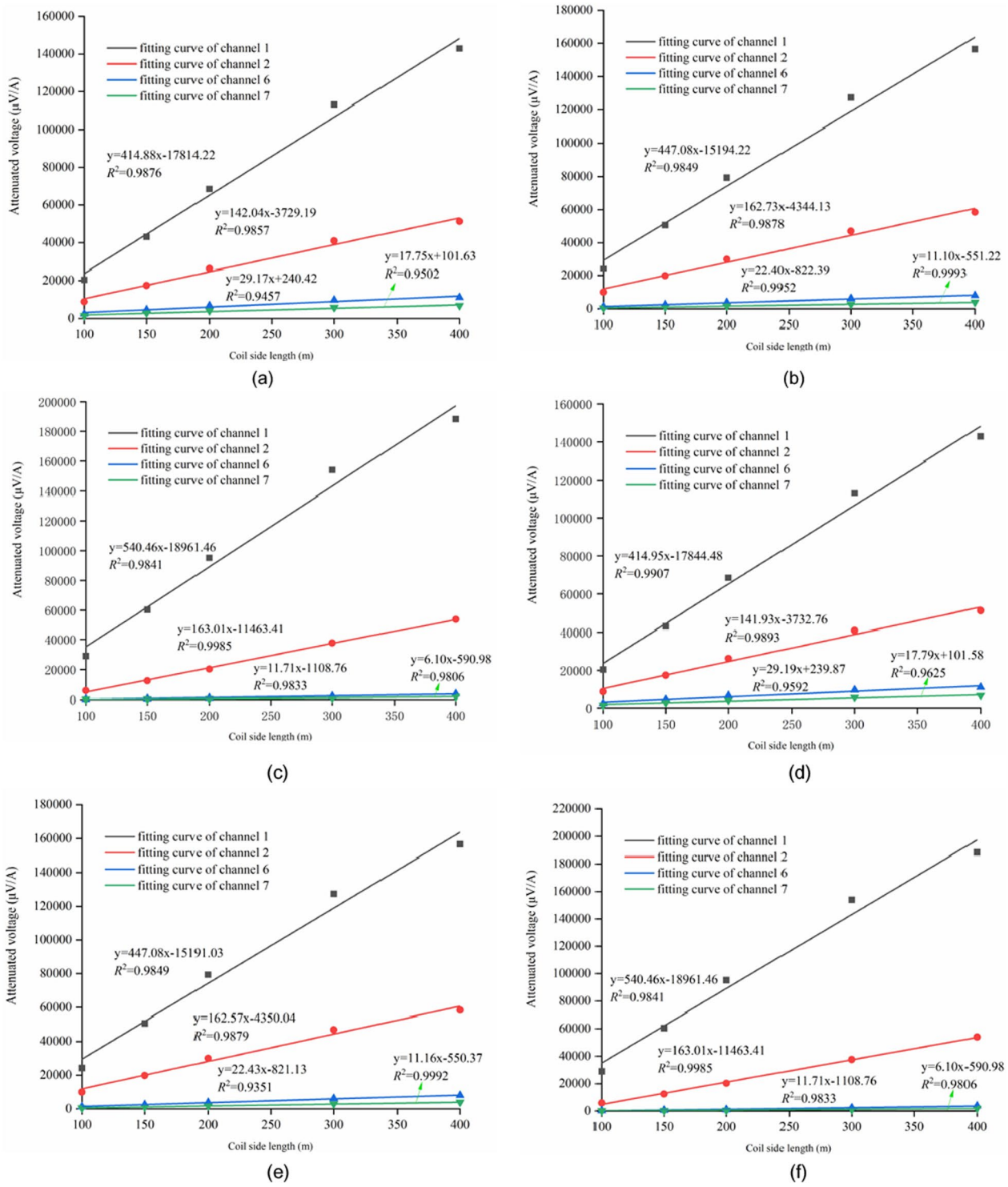

Fig. 9 Fitting curves of the attenuation voltage of the different models: **a** Model of the 100% water accumulation goaf; **b** Model of the 50% water accumulation goaf; **c** Model of the 0% water accumulation goaf; **d** Model of the 100% water accumulation with collapsed rock goaf; **e** Model of the 50% water accumulation with collapsed rock goaf; **f** Model of the 0% water accumulation with collapsed rock goaf

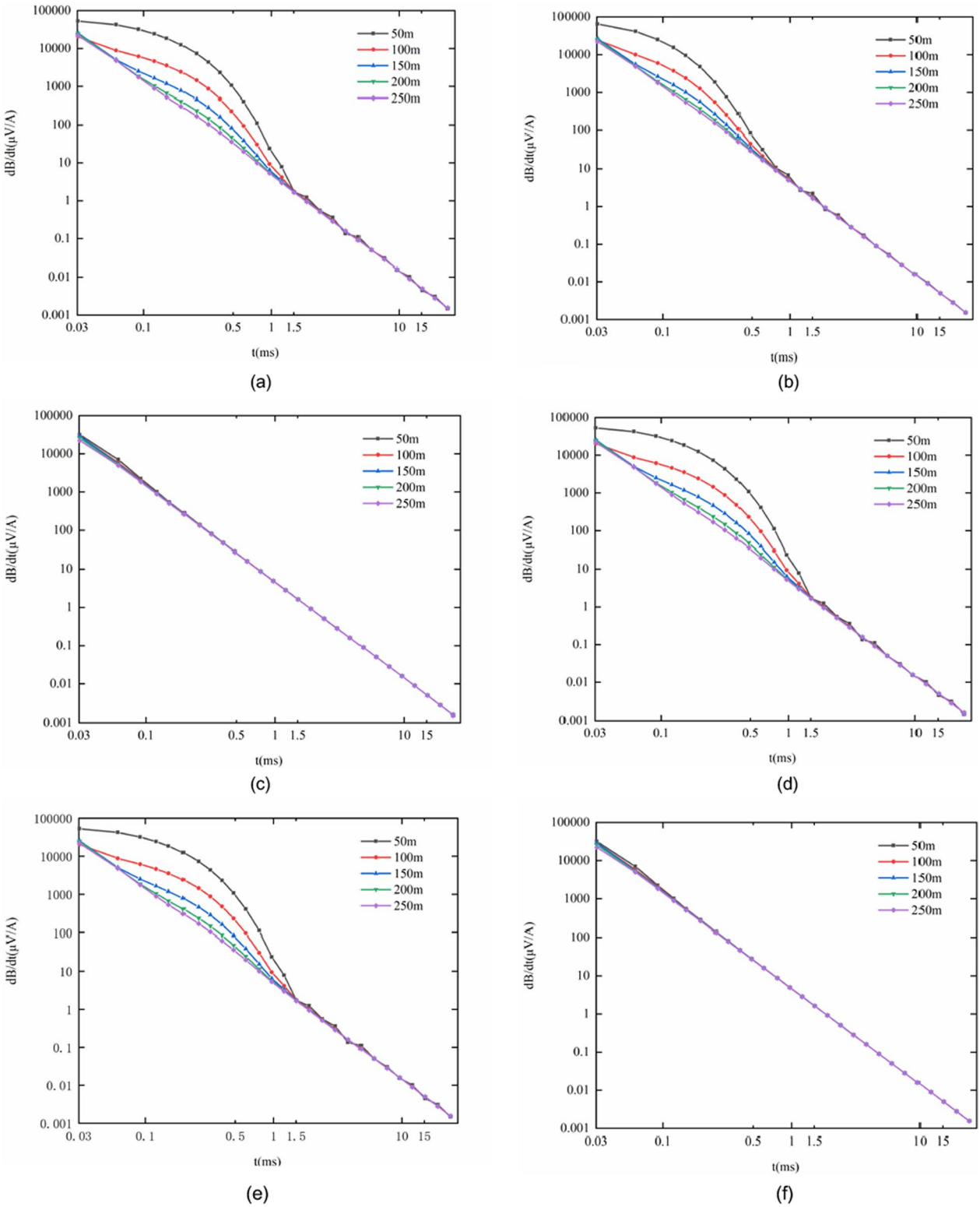

Fig. 10 Attenuated voltage curves of the different water-filled goaf models with different burial depths: **a** Model of the 100% water accumulation goaf; **b** Model of the 50% water accumulation goaf; **c** Model of the 0% water accumulation goaf; **d** Model of the 100% water accumulation with collapsed rock goaf; **e** Model of the 50% water accumulation with collapsed rock goaf; **f** Model of the 0% water accumulation with collapsed rock goaf

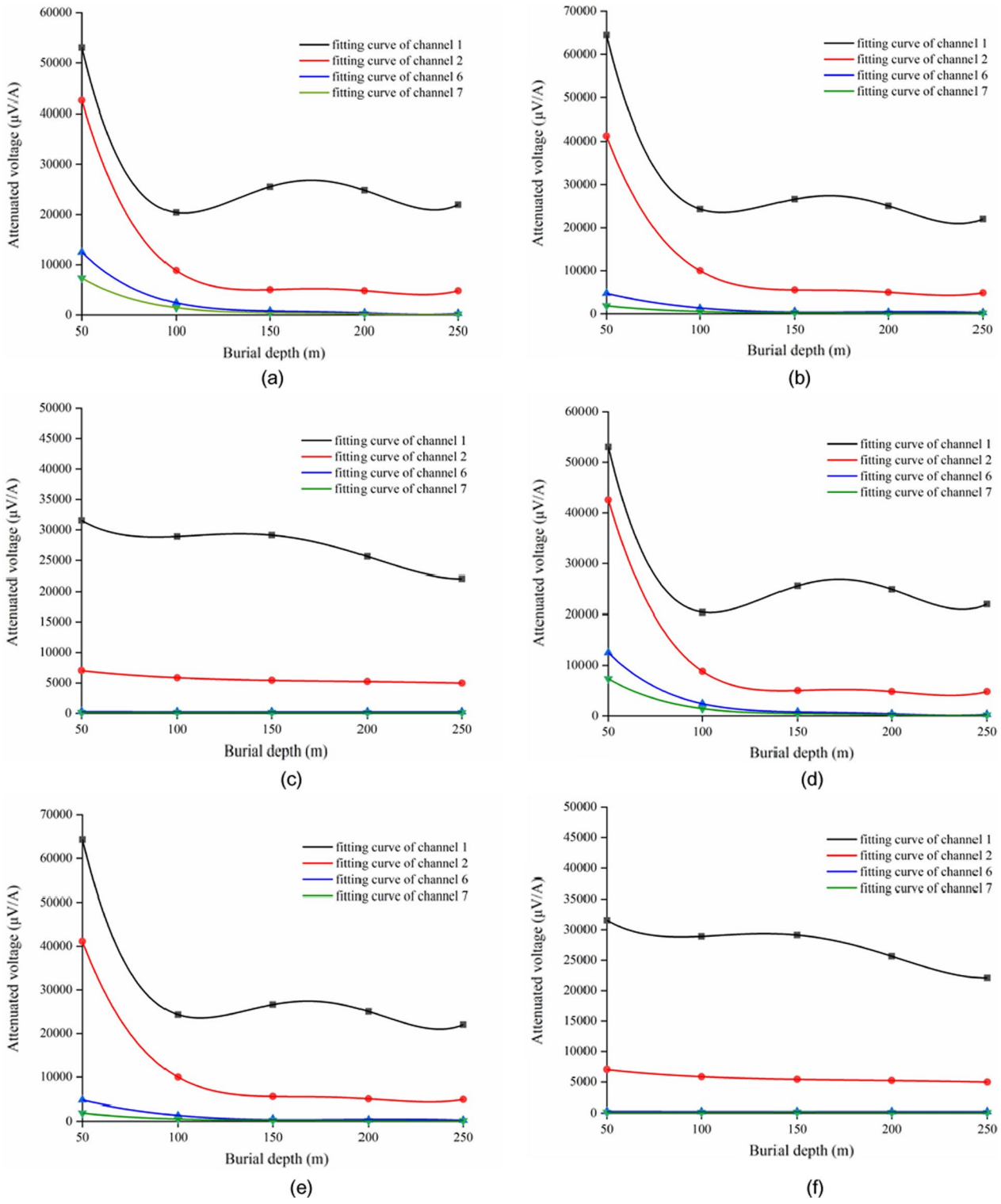

Fig. 11 Fitting curves of the attenuation voltage of with different burial depths: **a** Model of the 100% water accumulation goaf; **b** Model of the 50% water accumulation goaf; **c** Model of the 0% water accumulation goaf; **d** Model of the 100% water accumulation with collapsed rock goaf; **e** Model of the 50% water accumulation with collapsed rock goaf; **f** Model of the 0% water accumulation with collapsed rock goaf

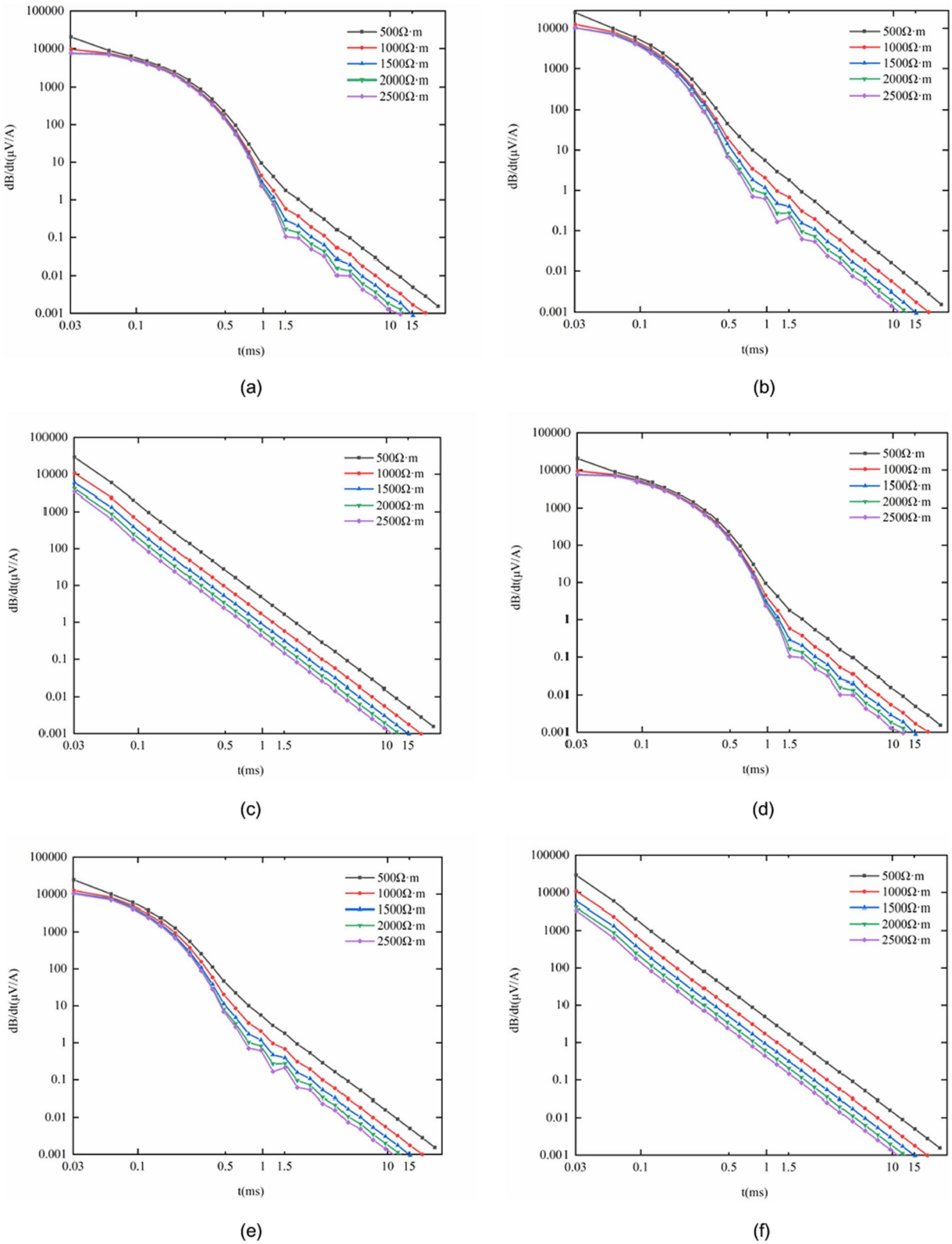

Fig. 12 Attenuated voltage curves of the different water-filled goaf models with different background resistivity: **a** Model of the 100% water accumulation goaf; **b** Model of the 50% water accumulation goaf; **c** Model of the 0% water accumulation goaf; **d** Model of the 100% water accumulation with collapsed rock goaf; **e** Model of the 50% water accumulation with collapsed rock goaf; **f** Model of the 0% water accumulation with collapsed rock goaf

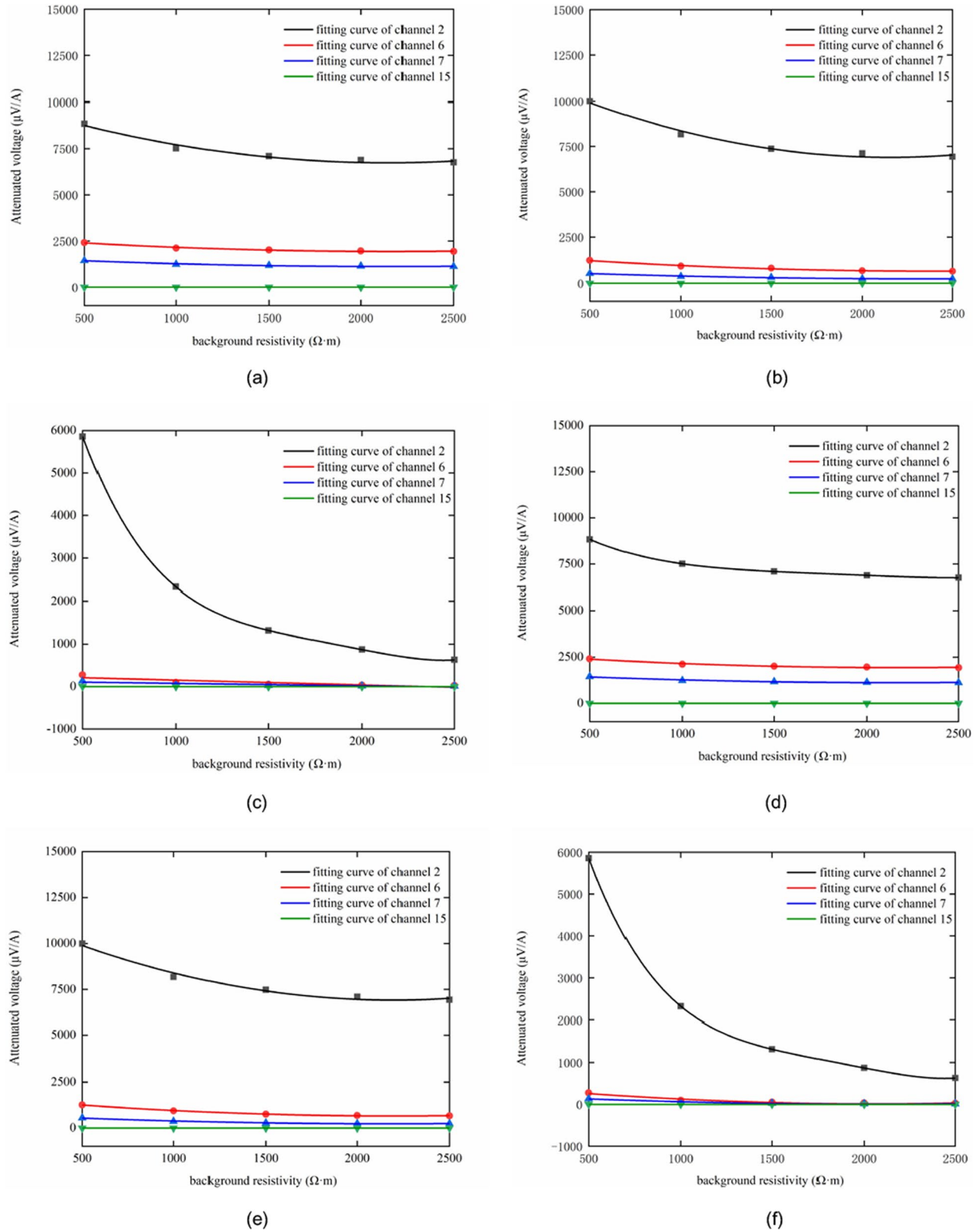

Fig. 13 Fitting curves of the attenuation voltage of with different background resistivity: **a** Model of the 100% water accumulation goaf; **b** Model of the 50% water accumulation goaf; **c** Model of the 0% water accumulation goaf; **d** Model of the 100% water accumulation with collapsed rock goaf; **e** Model of the 50% water accumulation with collapsed rock goaf; **f** Model of the 0% water accumulation with collapsed rock goaf

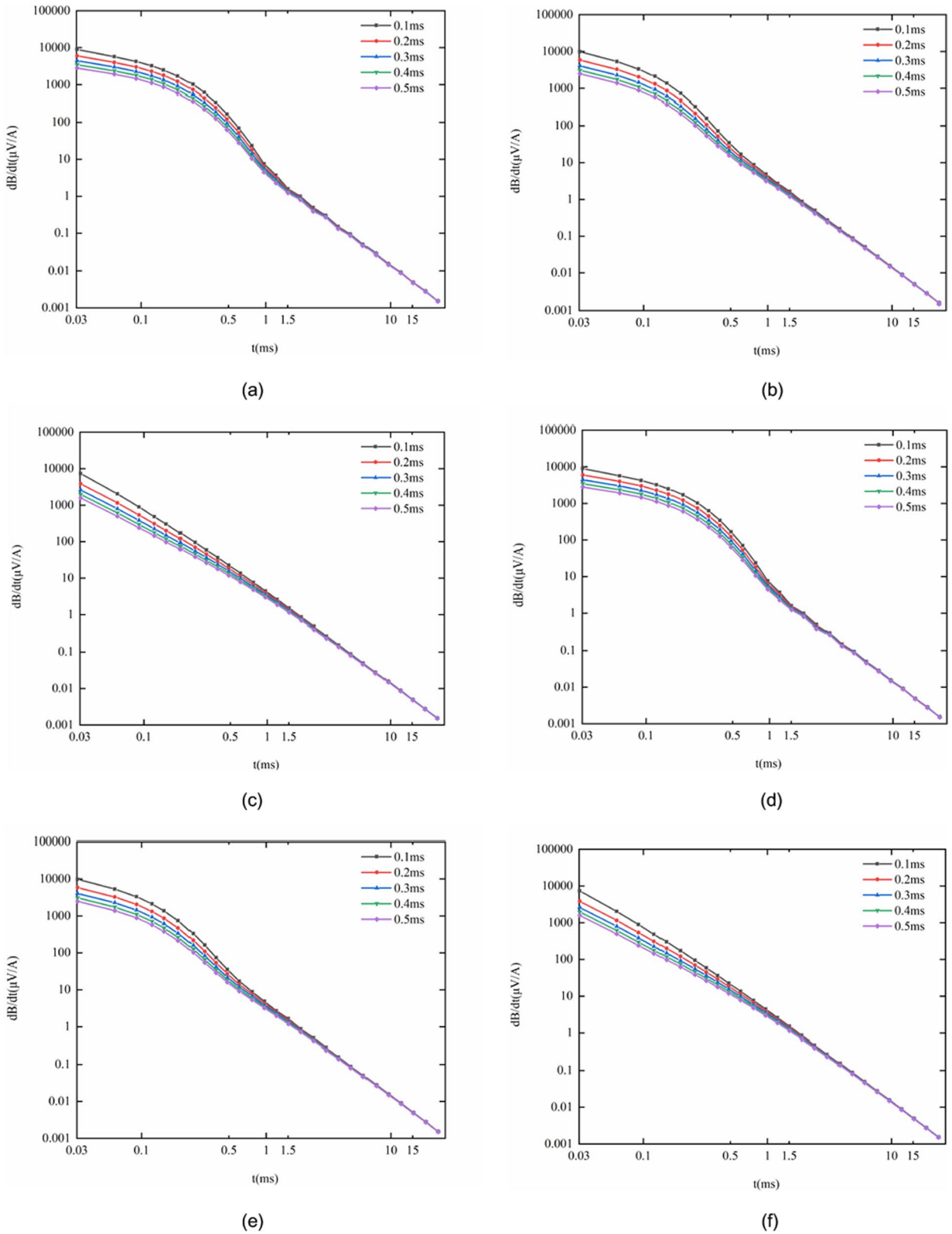

Fig. 14 Attenuated voltage curves of the different water-filled goaf models with different delay time: **a** Model of the 100% water accumulation goaf; **b** Model of the 50% water accumulation goaf; **c** Model of the 0% water accumulation goaf; **d** Model of the 100% water accumulation with collapsed rock goaf; **e** Model of the 50% water accumulation with collapsed rock goaf; **f** Model of the 0% water accumulation with collapsed rock goaf

is located directly above the center of the goaf, when there is water in the goaf, the attenuation voltage curve mainly reflects the low resistivity characteristics of the goaf, while when there is no water in the mining area, the attenuation voltage curve reflects the resistivity of the background.

3.7 Transient electromagnetic response characteristics of water-filled goaf with different delay time

This section studies the electromagnetic response characteristics of six goaf models with different delay time. The working parameters are set as follows: the emission current is 1 A, the emission frequency is 8 Hz, the number of turns is 1, the sampling time is 27 ms, and the number of time channels is 27, the buried depth of the water-filled goaf is 100 m, the background resistivity is 500 Ω m. We choose a 100 m × 100 m square coil for the transmitting coil, and a probe with an equivalent area of 10,000 m^2 for the receiving coil. The delay time is set as 0.1, 0.2, 0.3, 0.4 and 0.5 ms to perform forward calculations on each goaf model, as shown in Fig. 14.

From Fig. 14, it can be seen that in the early part of the attenuation voltage curve, regardless of whether there is water in the goaf, the shorter the delay time the greater the attenuation voltage value.In addition, a shorter delay time results in a more obvious abnormal bulge in the attenuation voltage curve of the water-accumulating goaf as shown in Fig. 14a, b, d and e, which helps in the identification of the water-accumulating goaf. At the last stage of the attenuation voltage curve, the effect of the delay time on the attenuation voltage value is small.

In order to obtain the relationship between the delay time and the attenuation voltage value, the second, fourth, sixth and seventh measurement channels of voltage values were selected to fit the relationship between the two, and the corresponding fitting curve is shown in Fig. 15. It can be seen that for different goaf, the response voltage value increases with the shortening of delay time, and the increase in the early measurement channel is more obvious.

4 Field application

4.1 Geological conditions of the mining area

The Majiliang Coalfield is located in the west of the Jurassic boundary of the Datong Coalfield, and belongs to the central and western wing of the Datong syncline (Fig. 16). The exploration area is the Carboniferous the No. 8 coal seam, which is located in the lower part of the Taiyuan Formation, generally about 15 m from the bottom of the K2 sandstone, and 18 m from the No. 5 coal seam. The thickness of the coal seam is 1.25–18.77 m, with an average of 8.38 m. The No. 8 coal seam is stable and simple in structure and contains 0–2 layers of gangue. In the eastern part of the mine field, it suffers from lamprophyre intrusion and damage to the coal seam, which has a large impact area. Also, it is one of the main mineable and stable coal seams in this area. Due to the small-scale coal mining excavation in the early stage, the location of the mining area and the water accumulation situation are uncertain. Therefore, the scope of the goaf of water accumulation should be explored.

4.2 Probe preparation and instrument selection

In this field experiment, the V8 multifunctional transient electromagnetic system was selected for ground transient electromagnetic detection. According to the actual geological conditions of the Majiliang mining area and multiple parameter optimization tests, we determined the final working parameters. The transient electromagnetic transmitter adopts T-4Amp, the coil is a square coil with a side length of 300 m, and the receiving device is replaced by a receiving coil with an equivalent area of 100 m^2. The operating frequency is 25 Hz, the transmitting current is 9 A, and the gain is 1. The prospecting area distributed on the 8111 working face on the southeast side of the mining area, and the survey area is about 1.21 km^2.

The experiment uses a 20 m × 20 m network type (which the line spacing is 20 m, and the point spacing is 20 m) to lay out the survey lines and points. A total of 3536 measurement points is arranged on the 8111 working face to ensure uniform coverage of the entire measurement area. Meanwhile, according to the information provided by the mine, the location of the predicted water-filled goaf was analysed and generated the site layout of the 8111 working face as shown in Fig. 17. The green box represents the detection coil, the internal numbers indicate the detection sequence, the pink dotted line represents the entire transient electromagnetic exploration boundary, the red cross represents the location of the measurement point, the black dotted line represents the coal seam boundary, and the number on the frame of the map represents the coordinate value of the mining area.

4.3 Results and analysis

After forward calculation and noise reduction processing, the attenuation voltage curves of the three regions are obtained, and corresponding to the region called L8-1, L8-2, and L8-3 as shown in Fig. 18. Among them, curves L8-2 and L8-3 have a “bulge” phenomenon at the sampling time of 0.27–2.28 ms. The voltage response value rises sharply during this period, indicating that the two curves are affected by the low resistivity abnormal effect and hinder the normal attenuation process. At the same time, the

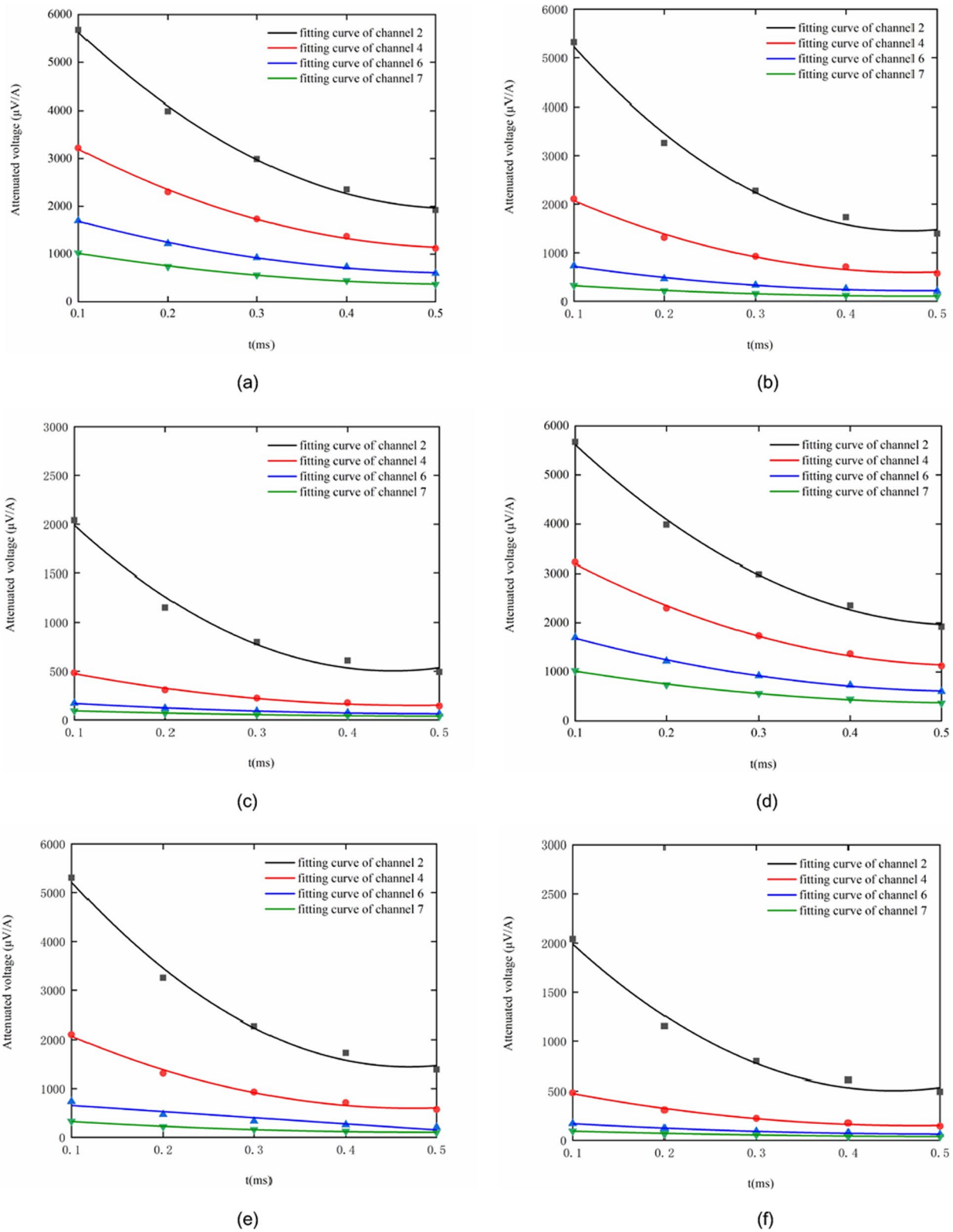

Fig. 15 Fitting curves of the attenuation voltage of with different delay time: **a** Model of the 100% water accumulation goaf; **b** Model of the 50% water accumulation goaf; **c** Model of the 0% water accumulation goaf; **d** Model of the 100% water accumulation with collapsed rock goaf; **e** Model of the 50% water accumulation with collapsed rock goaf; **f** Model of the 0% water accumulation with collapsed rock goaf

Fig. 16 Ground condition of 8111 working face

sequence of the abnormal amplitude about the three curves is L8-3 > L8-2 > L8-1, while the voltage response value during the abnormal time also follows the above relationship.

In line with the attenuation voltage curve under different water accumulation conditions of goaf obtained by numerical simulation and theoretical calculation, it can be inferred that the area where L8-2 and L8-3 located is water-filled goaf, and the area where L8-1 located is water-unfilled goaf. And the water accumulation degree in the area where the curve L8-3 is located is greater than that of the curve L8-2.

Based on the above forward simulation results, the apparent resistivity cross-section of the No. 8 coal seam in the 8111 working face is drawn in Fig. 19. The numbers outside the block diagram are the position coordinates of the detection area. The blue to red in the figure indicates that the apparent resistivity decreases from low to high, and blue relatively low-apparent resistivity area represents the range of water-filled goaf (excluding high-voltage line interference area). Meanwhile, 70 Ω m is used as the threshold for the low-value abnormality of apparent resistivity. The figure divides three low-resistivity areas, where numbered L8-1, L8-2, and L8-3. In addition, the cross-sectional diagram of apparent resistivity vs. depth of the L8-1, L8-2, L8-3 areas are shown in Fig. 20. It can be seen from the figure that the area and amount of accumulated water in the L8-3 area are the largest, the second is L8-2. The area of L8-1 is smaller and the amount of water contained in the former is negligible. It is inferred that there is no accumulated water in the mined area of L8-1. At last, the accuracy of the detection results was also verified after drilling.

5 Conclusions

(1) Based on Maxwell's equations, the transient electromagnetic detection theory of the goaf with water accumulation is derived, and the expression of the induced electromotive force is obtained. At the same time, Matlab software is used to calculate the change characteristics of the attenuation voltage response curve of the goaf with different water accumulation.

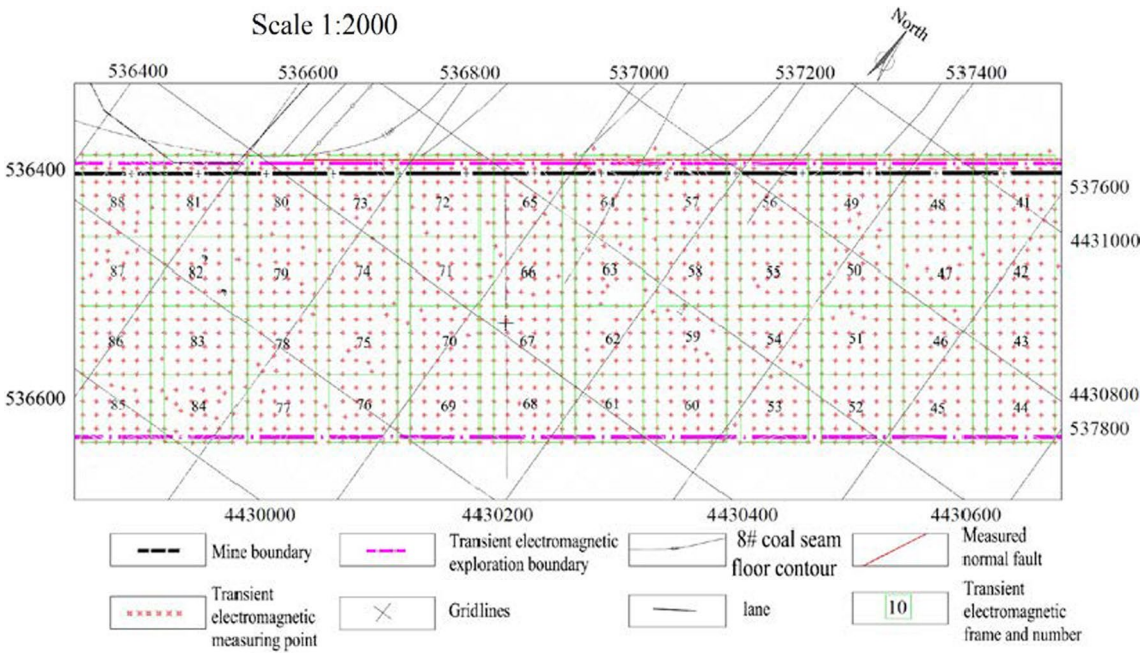

Fig. 17 Layout drawing of site detection on 8111 working face

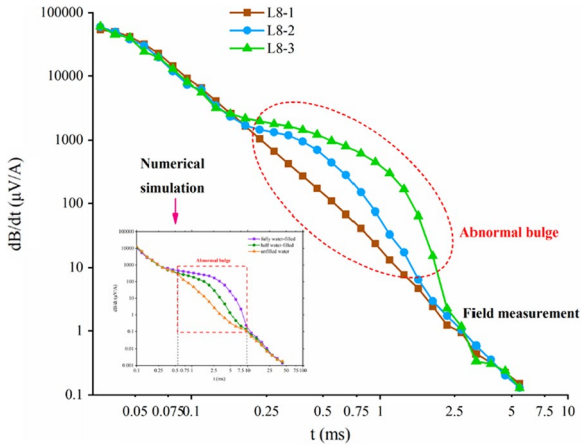

Fig. 18 Attenuation voltage curves under different measurement locations on 8111 working face and comparison analysis chart with numerical simulation

$$\frac{\partial B_z(t)}{\partial t} = \mu \frac{\partial H_z(t)}{\partial t} = \frac{3I_0\rho_w(3-\omega)}{2\omega a^3} \left[\Phi(u) - \sqrt{\frac{2}{\pi}}u\left(1+\frac{u^2}{3}\right)e^{-\frac{u^2}{2}}\right]$$

(2) According to the geology background of the Majiliang Coal Mine, goaf model with six water accumulation situation were built as 100% water accumulation, 50% water accumulation, 0% water accumulation, 100% water accumulation with collapsed rock, 50% water accumulation with collapsed rock and 0% water accumulation with collapsed rock goaf models. The simulation results demonstrate that the TEM detection has strong resolution in the low-resistivity water-filled goaf and would generate obvious abnormal reactions. The attenuation curve presents a third-order exponential function distribution, and the distribution form is "S". However, the resolution of the goaf without water content is poor, and there is no abnormality in the curve during the decay process, which follows the normal exponential decay pattern. At the same time, the larger the water accumulation could lead to higher the abnormal amplitude and greater the voltage response value. The collapsed rock wound slightly weaken the low-resistivity anomaly effect in the water-accumulated mine-out area.

(3) The transient electromagnetic response voltage decreases with increasing depth and background resistivity of the goaf. The depth of transient electromagnetic detectable goaf is not infinite, so it is important to study the influence of the burial depth of the goaf on the transient electromagnetic response characteristics for the accurate detection of large burial depth of the goaf. The background resistivity value has a great influence on the propagation and attenuation of electromagnetic field, so it is also meaningful to study the influence of the background field resistivity value on the transient electromagnetic response characteristic.

In addition, whether the goaf can be accurately detected is not only related to the geological condi-

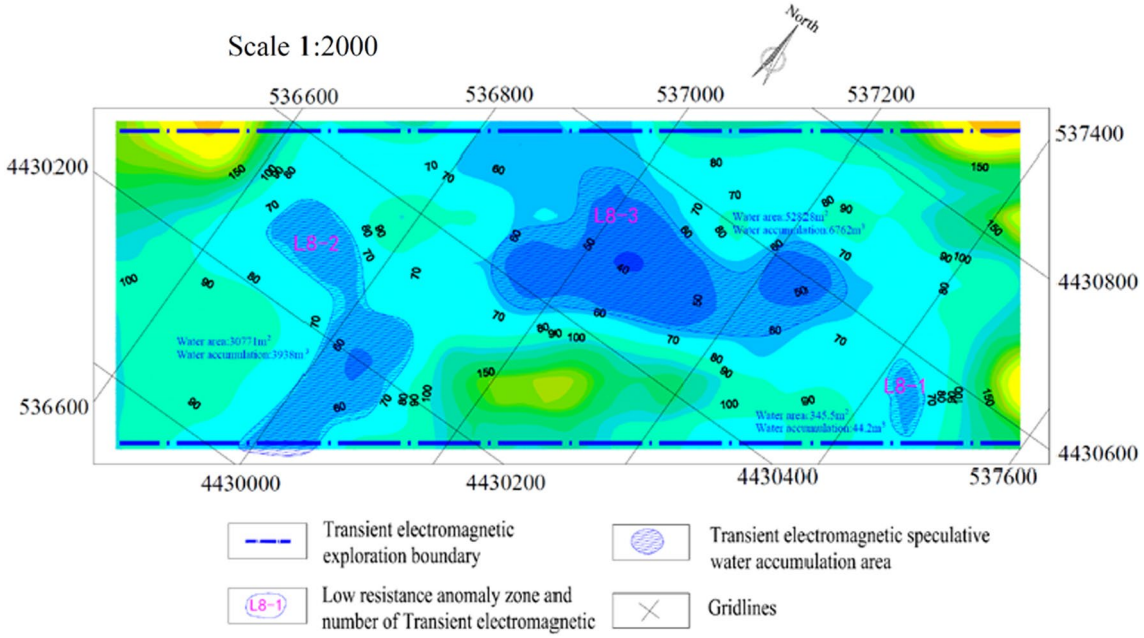

Fig. 19 Apparent resistivity profile of the No. 8 coal seam on 8111 working face

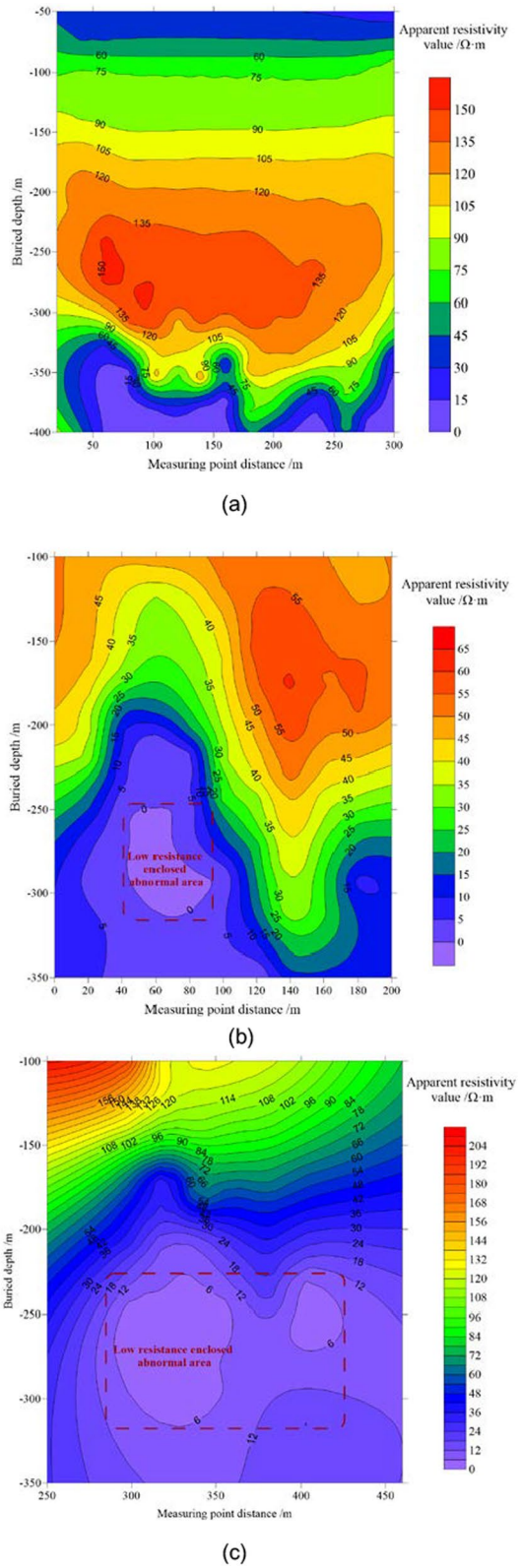

Fig. 20 Cross sectional diagram of apparent resistivity versus depth. **a** The area of L8-1. **b** The area of L8-2. **c** The area of L8-3

tions, but the parameter settings of the instrument also have a significant impact on the transient electromagnetic detection. Through the study of this paper, it is found that when the side length of the transmitting coil increases or the delay time decreases, the response voltage value increases. The side length of the transmitting coil determines the range of the transient electromagnetic field, while the delay time affects the intensity of the transient electromagnetic field. Therefore, the study of both has an important impact on the accurate exploration of the goaf.

(4) The results of the attenuation curve of theoretical analysis and numerical simulation were verified through field detection experiment of Majiliang coal mine. Meanwhile, the research results of this paper provide theoretical and technical guidance for the accurate detection and effective treatment of water-filled goaf.

Acknowledgements The project was supported by the Joint Funds of National Natural Science Foundation of China and Shanxi Province (U1710258 and U1810120), Distinguished Youth Funds of National Natural Science Foundation of China (51925402), Ten Thousand Talent Program of China for Leading Scientists in Science, Technology and Innovation, Shanxi Science and Technology Major Project Funds (No. 20201102004), Shanxi "1331 Project" Funds, Shanxi Province Key Laboratory Construction Project Funds (No. 202104010910021), Shanxi-Zheda Institute of Advanced Materials and Chemical Engineering (No. 2021SX-TD001, No. 2021SX-TD002) and National Natural Science Foundation of China (51804208).

Declarations

Conflict of interest The authors declare that they have no conflict of interest.

References

Abu Rajab JS, El-Naqa AR (2013) Mapping groundwater salinization using transient electromagnetic and direct current resistivity methods in Azraq Basin, Jordan. Geophysics 78:B89–B101

Bai DH, Meju MA, Lu J, Wang LF, He ZH (2003) Numerical calculation of all-time apparent resistivity for the central loop transient electromagnetic method. Chin J Geophys 46(5):697–704

Chang JH, Yu JC, Su BY (2017) Numerical simulation and application of mine TEM detection in a hidden water-bearing coal mine collapse column. Environ Eng Geophys 22(3):223–234

Chang JH, Su BY, Malekian R (2019) Detection of water-filled mining goaf using mining transient electromagnetic method. IEEE Trans Ind Inform 99:1–1

Constable SC, Parker RL, Constable CG (1987) Occam's inversion: a practical algorithm for generating smooth models from electromagnetic sounding data. Geophysics 52(3):289–300

Dong SN (2007) Coal mine water hazard prevention technology and application, safety and efficient coal mine geological support technology and application. In: China coal industry labor protection science and technology society water hazard prevention committee proceedings of the academic annual conference. China Geological Society, China Coal Society Coalfield Geology Committee, Beijing

Fitterman DV, Menges CM, Aikamali AM, Jama FE (1991) Electromagnetic mapping of buried paleochannels in eastern Abu Dhabi Emirate, UAE. Geoexploration 27(1–2):111–133

Garg NR, Keller GV (1999) Spatial and temporal analysis of electromagnetic survey data. Geophysics 51(1):85–89

Han Y (2018) The research on abnormal range of central loop by transient electromagnetic method. Taiyuan University of Technology, Taiyuan

Hou EK, Wen Q, Ye ZN, Chen W, Wei JB (2020) Height prediction of water-flowing fracture zone with a genetic-algorithm support-vector-machine method. Int J Coal Sci Technol 7(4):740–751. https://doi.org/10.1007/s40789-020-00363-8

Jiang ZH, Yang G (2014) Research and application of TEM detection technology for small mine gob area in shallowly-buried and extremely thick seam. J Min Saf Eng 31(5):769–774

Li Y (2002) The theory and application of transient electromagnetic sounding. Shaanxi Science and Technology Press, Xi'an

Li CY, Liu HF (2007) The application of transient electromagnetic method to the detection of multilayer worked-out area of coal seam. Geophys Geochem Explor 31(S1):108–110

Lian XG, Hu HF, Li T, Hu DS (2020) Main geological and mining factors affecting ground cracks induced by underground coal mining in Shanxi Province, China. Int J Coal Sci Technol 7(2):362–370. https://doi.org/10.1007/s40789-020-00308-1

Liu SD, Liu J, Yue JH (2014) Development status and key problems of Chinese mining geophysical technology. J China Coal Soc 39(1):19–25

Luo HG (2012) The study about 1D Forward modeling of large-fixed loop TEM. China University of Geosciences, Beijing

Shan L, Xu RK, Lu SZ, Li XD, Cao CG, Zhang YL, Cao L (2009) The transient electromagnetic method: principle, current situation and application in mineral exploration. Geol Resour 18(1):70–73

Tang ZY, Zhang H, Gong YL (2015) The application of transient electromagnetic imaging technology to goaf water. Chin J Eng Geophys 12(5):633–636

Taylor K, Widmer M, Chesley M (1992) Use of transient electromagnetic to define local hydrogeology in an arid alluvial environment. Geophysics 57:343–352

Tong XZ, Liu JX (2013) MATLAB programming and its application in geophysics. Central South University Press, Changsha

Wang P, Cheng JY, Yao WH, Li MX, Wang Y (2019) Technology of detecting water-filled goaf beside borehole using downhole transient electromagnetic method. J China Coal Soc 44(8):2502–2508

Yan GC, Xian PH, Qiu NG (2020) Study on short offset transient electromagnetic detection technology for low-resistance electrical sources in deep mine. Coal Sci Technol 48(6):171–176

Yu CT, Liu XY, Liu JS (2018) Application of transient electromagnetic method for investigating the water-enriched mined-out area. Appl Sci 8(10):1800–1811